

Bioapatite crystallinity and Rare Earth Element signatures in fossil and Recent sharks: A window into Past and Present seas

Luca Medici^a, Annalisa Ferretti^{b,*}, Alberto Collareta^c, Giulia Bosio^c, Giovanni Bianucci^c, Giorgio Carnevale^d, Simone Casati^{e,f}, Simona Clò^g, Luca Lanteri^h, Federico Lugli^b, Giuseppe Marramà^d, Frederik H. Mollenⁱ, Martina Savioli^b, Daniele Malferrari^b

^a National Research Council of Italy, Institute of Methodologies for Environmental Analysis, C. da S. Loja-Zona Industriale, 85050 Tito Scalo, Potenza, Italy

^b Department of Chemical and Geological Sciences, University of Modena and Reggio Emilia, via Campi 103, 41125 Modena, Italy

^c Department of Earth Sciences, University of Pisa, via S. Maria 53, 56126 Pisa, Italy

^d Department of Earth Sciences, University of Turin, via Valperga Caluso 35, 10125 Turin, Italy

^e GAMPs Geopaleontological Museum, Piazza Vittorio Veneto 1, Badia a Settimo, 50018 Scandicci, Florence, Italy

^f Institute of Applied Physics "Nello Carrara", CNR-IFAC, via Madonna del Piano 10, 50019 Sesto Fiorentino, Florence, Italy

^g MedSharks, via di Casalotti 318, 00166 Roma, Italy

^h Department of Earth, Environmental and Life Science (DISTAV), University of Genoa, Corso Europa 26, 16132 Genova, Italy

ⁱ Elasmobranch Research Belgium, Rehaegenstraat 4, 2820 Bonheiden, Belgium

ARTICLE INFO

Editor: Christian France-Lanord

Keywords:

Calcium phosphate
Diagenesis
Scyliorhinidae
Crystallinity Index
REE

ABSTRACT

The advent of biomineralization represented a key evolutionary innovation, enabling vertebrates to form skeletons and teeth made of bioapatite, a nanocrystalline apatite phase with variable chemical composition. This adaptability has driven vertebrate morphological diversity and ecological success. Bioapatite structure is shaped by metabolic processes, with ionic substitutions and vacancies influencing its crystallographic parameters. Major elements alter the *a* and *c* parameters of the bioapatite cell, while trace elements have minimal impact. Rare Earth Element (REE) signatures in fossil bioapatite, once considered direct proxies for paleo-seawater, may reflect complex diagenetic histories. This study examines bioapatite crystallinity and REE patterns in Recent and fossil catsharks (*Scyliorhinidae s.l.*) using μ -XRD and LA-ICP-MS. Recent teeth and scales of *Galeus melastomus* and *Scyliorhinus canicula* from the Italian coasts were tested and compared with fossil Eocene to Pliocene counterparts from strata across Europe. Our results underscore the value of crystallographic parameters in tracing both biological and *post-mortem* transformations in bioapatite. In particular, diagenetic processes led to organic matter loss and increased carbon incorporation, especially in tooth regions that were originally rich in organics. Fossil samples showed reduced *a* lattice parameters and unit cell volumes, increased *c* parameters, and enhanced crystallinity. Tooth crowns had higher crystallinity and volume than roots, reflecting lower organic contents. Crystallographic differences between scales and teeth suggest functional adaptations, with teeth exhibiting variable crystallite sizes for biomechanical efficiency. Diagenetic effects are seemingly independent of geological age, being rather influenced by depositional conditions and, possibly, by original physiological traits.

1. Introduction

Biomineralization triggered a fundamental evolutionary step in the history of life. By acquiring a rigid framework, organisms were indeed able to experiment with novel architectures and develop unprecedented

functional capabilities. The newly invented hard parts were comprised of a delicate association between an organic matrix and an inorganic mineral phase. Different animal groups experimented diverse mineral substances associated with different organic scaffolds (*i.e.*, biominerals). These organic components are not uniform across taxa: their abundance,

* Corresponding author.

E-mail addresses: E-mail addresses: luca.medici@cnr.it (L. Medici), ferretti@unimore.it (A. Ferretti), alberto.collareta@unipi.it (A. Collareta), giulia.bosio.giulia@gmail.com (G. Bosio), giovanni.bianucci@unipi.it (G. Bianucci), giorgio.carnevale@unito.it (G. Carnevale), sim.casati@gmail.com (S. Casati), simona@medsharks.org (S. Clò), luca.lanteri@libero.it (L. Lanteri), federico.lugli@unimore.it (F. Lugli), giuseppe.marrama@unito.it (G. Marramà), frederik.mollen@gmail.com (F.H. Mollen), martina.savioli.17@gmail.com (M. Savioli), daniele.malferrari@unimore.it (D. Malferrari).

<https://doi.org/10.1016/j.chemgeo.2025.123200>

Received 25 October 2025; Received in revised form 7 December 2025; Accepted 9 December 2025

Available online 10 December 2025

0009-2541/© 2025 The Author(s). Published by Elsevier B.V. This is an open access article under the CC BY license (<http://creativecommons.org/licenses/by/4.0/>).

molecular composition, and structural organization differ among groups, influencing eventually how biominerals respond to diagenetic alterations (Weiner and Dove, 2023). Calcium carbonates and silica are the most common mineral phases among invertebrates, while vertebrates preferred to rely on calcium phosphate (*i.e.*, bioapatite) to build their bones and teeth (see, among others, Lowenstam and Weiner, 1989; Benton and Harper, 2009). Thanks to its remarkable plasticity, the vertebrate skeleton can be regarded as the main responsible for the origin of a cornucopia of structures and body plans, which in turn resulted in the outstanding evolutionary and ecological success of vertebrates (Shirley et al., 2024).

Bioapatite is a nanocrystalline phase characterized by a variable chemical composition, stemming from ionic substitutions and vacancies within its structure. *In-vivo* metabolic processes modulate its chemical composition and crystal architecture, facilitating adaptation to specific physiological functions (Dal Sasso et al., 2018). Although the fundamental hexagonal crystal structure remains unaltered by these compositional changes, which include both major and trace elements, they still have different effects on lattice parameters. Specifically, major element substitutions can affect the length of the *a* and *c* cell parameters, while trace element substitutions typically do not significantly impact on them due to their low concentrations. Regardless of this, the concentrations and interrelationships of Rare Earth Elements (REE) and other High Field Strength Elements (HFSE) have been widely utilized to infer the original seawater composition recorded by fossil bioapatite. In addition to REE and HFSE systematics, the stable isotope composition of shark tooth bioapatite has also been used as a proxy for environmental conditions in modern and fossil settings (see, *e.g.*, Vennemann et al., 2001; Fischer et al., 2013). Early studies (*e.g.*, Wright et al., 1984; Grandjean et al., 1987; Grandjean-Lécuyer et al., 1993; Girard and Albarède, 1996; Pietsch and Bottjer, 2010; Song et al., 2019) largely considered REE and other HFSE in bioapatite to be reliable archives of marine conditions at the time of deposition. Within this framework, bioapatite was thought to directly acquire a hydrogenous REE signature from seawater, which is typically characterized by low total REE contents and a distinct depletion in light REEs (Webb and Kamber, 2000; Lécuyer et al., 2004; Nothdurft et al., 2004; Webb et al., 2009). However, from the 1990s onward, new studies suggested that REE and HFSE concentrations in bioapatite might be significantly modified by *post-mortem* processes, which are particularly influenced by the chemical and mineralogical properties of the diagenetic environment (Toyoda and Tokonami, 1990; Holser, 1997; Reynard et al., 1999; Armstrong et al., 2001; Vennemann et al., 2001; Picard et al., 2002). These concerns have since been corroborated by further research (*e.g.*, Trotter and Eggins, 2006; Kocsis et al., 2010; Herwartz et al., 2011, 2013; Zhao et al., 2013; Chen et al., 2015; Trotter et al., 2016; Zhang et al., 2016; Liao et al., 2019; Žigaitė et al., 2020; Bosio et al., 2021). Nevertheless, despite the ongoing debate (Liao et al., 2019), there is a growing consensus that REE patterns in fossil bioapatite often reflect a diagenetic overprint rather than purely primary seawater composition (Lécuyer et al., 2004; Kim et al., 2012; Chen et al., 2015; Trotter et al., 2016). This shift has prompted some workers (*e.g.*, Zhang et al., 2016) to conclude that numerous studies interpreting bioapatite on the only basis of HFSE concentrations and REE anomalies warrant reconsideration. Within this framework, the uptake of REE during burial is predominantly governed by diagenetic processes. Such processes can impart a pore-water signature that frequently exceeds the original signal by several orders of magnitude (Pattan et al., 2005; Chen et al., 2015; Zhang et al., 2016). For instance, diagenetically influenced signatures commonly exhibit elevated Σ REE, pronounced thorium enrichment, and elevated LREEs (Wright and Colling, 1995; McLennan, 2001; Peppe and Reiners, 2007; Shen et al., 2012). Taken together, these findings indicate that REE signatures in fossil bioapatite, which were once considered straightforward indicators of seawater composition, are now understood to provide potentially complex records integrating both primary signals and substantial diagenetic modifications. Nevertheless, as previously mentioned,

crystal-chemical changes in bioapatite occurring during life and *post-mortem* can also be traced by considering the crystallographic parameters. Ferretti et al. (2021) have described the crystallographic signature of bioapatite in living, dead, and fossil remains of both vertebrate and invertebrate organisms, spanning over 500 million years (*i.e.*, from the Cambrian to the Recent). Their study shows that fossil bioapatite is characterized by lower values for the crystal lattice cell parameter *a*, while the cell parameter *c* is less variable. This results in a general decrease of the cell volume (*i.e.*, the volume of the hexagonal crystalline unit cell) over time, from living to fossil organisms. Bioapatite transformation over time can also be reflected by crystallinity, a parameter that indicates the degree of ordering within the crystal structure. Several empirical crystallinity parameters have been proposed, reflecting the diverse analytical techniques used for their measurement, such as X-ray powder diffraction (XRPD), Fourier transform infrared spectroscopy (FTIR), Raman spectroscopy, transmission electron microscopy (TEM), atomic force microscopy, and nuclear magnetic resonance (NMR) (Dal Sasso et al., 2018).

Here, we investigated bioapatite crystallinity in a carefully selected set of Recent and fossil catsharks (Elasmobranchii: Scyliorhinidae *sensu lato*) using X-ray microdiffraction (μ -XRD). REE signatures were concurrently measured. Catsharks were chosen due to their remarkable extant diversity (Froese and Pauly, 2024), deep paleontological record (Underwood, 2006), abundance of fossil representatives (Cappetta, 2012) and relevance as model taxa for tooth development studies (*e.g.*, Fraser and Hulsey, 2020), as well as for the non-threatened status of some of their commonest living representatives (IUCN, 2025), which allows for the sustainable sampling of a relatively high number of individuals. The study was conducted by a multidisciplinary team comprising specialists in extant and extinct sharks, chemists, crystallographers and geochemists. Its overarching objective was to identify how bioapatite crystallinity responds to fossilization, with the aim of identifying some specific diagenetic imprints preserved within the bioapatite crystal lattice as well as more general patterns that explain preservation across different taphonomic pathways. Our results appear to be particularly valuable as well as broadly applicable – not only to the study of sharks, both living and fossil, but more generally to vertebrate research.

2. Catsharks and their biomineralized products

2.1. Catsharks in time and space

The vernacular name “catsharks” applies to 18 genera and *ca.* 160 currently valid species of colorful, small-sized sharks that dwell near the bottom of almost all seas – from cold to tropical waters and from the intertidal zone to depths greater than 2000 m (Froese and Pauly, 2024). Catsharks account for about one-fourth of the extant shark species, with new species being described on a more-than-yearly basis (Weigmann, 2016). Catsharks have long been classified into the family Scyliorhinidae (*sensu Compagno, 1988*), and still are by some (*e.g.*, Bánki et al., 2024). However, a growing amount of research indicates that this family is paraphyletic (Iglésias et al., 2005), likely representing a grade toward the so-called “higher carcharhiniforms” (Soares and Mathubara, 2022 and references therein). Recently, the scyliorhinids (*s.l.*) have been classified into as many as four modern families, namely, Scyliorhinidae (*sensu stricto*), Pentanchidae, Atelomycteridae and Dichichthyidae (*e.g.*, White et al., 2024).

At present, catsharks are represented in the Mediterranean Sea by a handful of species, among which the most common and abundant are the small spotted catshark, *Scyliorhinus canicula* (Linnaeus, 1758), and the blackmouth catshark, *Galeus melastomus* Rafinesque, 1810 (Serena et al., 2020). These are demersal species that inhabit all the Italian seas, where they are found on sandy and muddy bottom, although the blackmouth catshark is rare in the northern and central Adriatic Sea (Vacchi and Serena, 2010), living as it does on the outer edge of the

continental shelf and slope (Abella et al., 2017a), while *S. canicula* inhabits most of the continental shelf as well as uppermost slope (Abella et al., 2017b). Both these species are commonly caught as by-catch of demersal fisheries, especially during trawling operations. However, due to their high abundance and low fishing mortality, they are classified as “Least Concern” in the most recent assessments of the IUCN committee (Finucci et al., 2021a, 2021b). In light of this, both species were sampled for teeth and scales (see Methods below).

As far as the fossil record is concerned, the earliest putative catsharks have been recognized in the form of teeth from deposits as old as the Middle Jurassic (Underwood, 2006). Complete, exceptionally preserved specimens from the Upper Jurassic Solnhofen Lagerstätte of Germany have been interpreted as representing scyliorhinids *s.l.* (e.g., Wagner, 1857; Thies, 2005), though this assignment remains somewhat contentious (Villalobos-Segura et al., 2023). Small, scyliorhinid-like taxa remained dominant among Carcharhiniformes until the Late Cretaceous, when the radiation of the higher carcharhiniforms began (Brée et al., 2022). In the present paper, the following extinct catshark-like taxa were scrutinized:

- (1) *Scyliorhinus woodwardi* Cappetta, 1976, a lower Eocene (Ypresian) species that is known primarily from the North Sea basin;
- (2) *Pachyscyllium distans* (Probst, 1879), an Oligocene to Pliocene member of the extinct subfamily Premontreinae that inhabited both sides of the North Atlantic as well as the Mediterranean and Paratethys basins (see Collareta et al., 2021b);
- (3) *Pachyscyllium dachiardii* (Lawley, 1876), a close ally of *P. distans*, with which it lived sympatrically in several localities;
- (4) *Megascyliorhinus miocaenicus* (Antunes and Jonet, 1970), an enigmatic Neogene species that may or may not represent an idiosyncratic catshark (see Manganelli and Spadini, 2019).

2.2. Catshark teeth and scales

Due to their common dermal origin, shark teeth and scales share the same overall structure, both being formed by a more organic-rich, bone-like bioapatite tissue (*i.e.*, dentine) topped by a thin layer of more compact, enamel-like bioapatite tissue (*i.e.*, the enameloid) (e.g., Cappetta, 2012; Enax et al., 2012; Bosio et al., 2022) (Fig. 1). In the case of teeth, the enameloid-coated, typically cuspidate tooth portion comprises the crown, which is supported by the enameloid-free root attaching to

the largely cartilaginous jaws. Similarly, the placoid scales of sharks feature a dentine trunk overlain by an enameloid crown. Regarding the tooth histology, three main tooth histotypes are recognized in sharks: orthodont, osteodont and pseudoosteodont (Glickman, 1964; Compagno, 1988; Cappetta, 2012; Jambura et al., 2018). Specifically, orthodont teeth retain an open pulp cavity surrounded by orthodentine; osteodont teeth are completely filled with osteodentine; and pseudoosteodont teeth exhibit secondary infilling of the pulp cavity by osteodentine (Ørvig, 1951; Moyer et al., 2015; Cuny et al., 2017; Jambura et al., 2018, 2020). As typical of Carcharhiniformes, scyliorhinid teeth belong in the orthodont histotype, although this has not been verified for all extant and extinct taxa, and the phylogenetic and histological affinities of *Megascyliorhinus* remain uncertain (Cione, 1986; Suarez et al., 2004; Cappetta, 2012). Regardless of these uncertainties, shark tooth roots are invariably comprised of osteodentine, which represents a porous, organic-rich, and overall bone-like variety of dentine (Berkovitz and Shellis, 2017).

3. Material and provenance

3.1. Recent sharks

The blackmouth catshark (*G. melastomus*) is a typically benthic species, living on the outer edge of the continental shelf and slope, down to 2000 m water depth (Finucci et al., 2021a, 2021b). In the Ligurian sea (Fig. 2), juveniles are more frequently encountered between 200 and 500 m water depth, while adults are mostly found between 500 and 800 m water depth (Pinto et al., 2010).

The small-spotted catshark (*S. canicula*) is a small eurybathic scyliorhinid distributed on the continental shelf and uppermost slope, from the coastal area to approximately 400 m water depth in the Atlantic Ocean (Compagno, 1984), and down to 800 m in the Eastern Mediterranean Sea (Mytilineou et al., 2005). Data from the Mediterranean International Trawl Survey (MEDITS) program indicates that this species occurs extensively throughout the northern Mediterranean Sea (Baino et al., 2001).

A total of 30 catshark specimens, including 21 individuals of *G. melastomus* and 9 individuals of *S. canicula*, were collected from two distinct areas in 2019 (Fig. 2; Tables 1 and 2). All the *G. melastomus* specimens were obtained from the landings of Ligurian bottom trawl

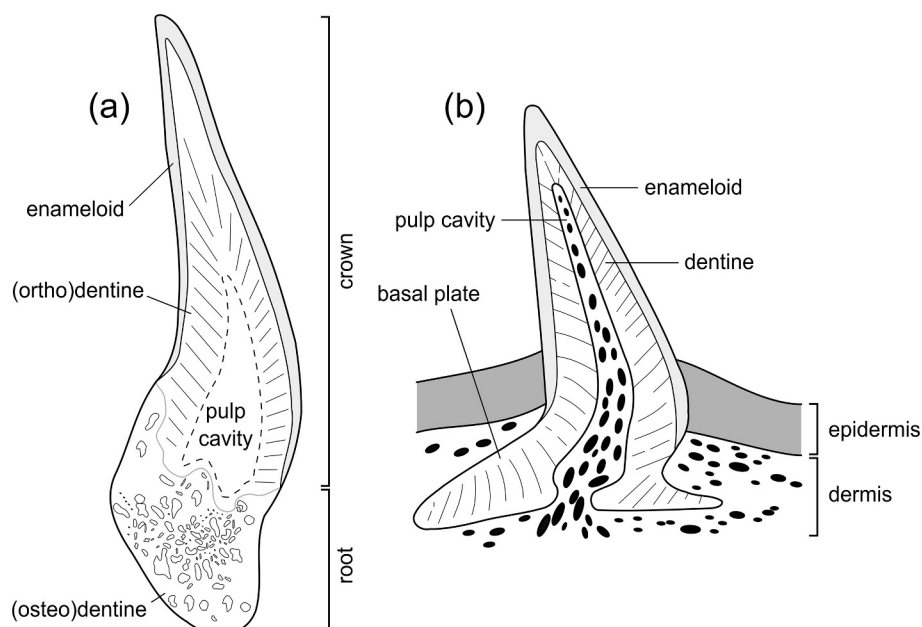


Fig. 1. Basic histological nomenclature for osteodont shark teeth (a) and placoid scales (b).



Fig. 2. Location map of the sites investigated in this paper. Black circles indicate Recent material, black squares indicate fossil samples. 1: Porto Savona (Italy); 2: Porto Santa Margherita Ligure (Italy); 3: Porto San Benedetto del Tronto (Italy); 4: Egem, West-Flanders (Belgium), lower Eocene, Ypresian; 5: Loupian, Hérault (France), Middle Miocene, Langhian; 6: Rapolano, Tuscany (Italy), Pliocene; 7: Arcille, Tuscany (Italy), Pliocene.

Table 1
Sampling sites of the Recent shark material investigated in the present study.

| TAXA | SAMPLING SITE | COORDINATES |
|------------------------------|---|-------------------------------|
| <i>Galeus melastomus</i> | Haul of Santa Margherita fishing vessel | N 44° 15.024' E 9° 10.159' |
| <i>Galeus melastomus</i> | Haul of Savona fishing vessel | N 44° 14.710' E 8° 41.330' |
| <i>Scyliorhinus canicula</i> | Haul of San Benedetto del Tronto fishing vessel | not available |

fisheries targeting the blue and red shrimp (*Aristeus antennatus*) and giant red shrimp (*Aristaeomorpha foliacea*), which are among the most commercially important deep-water species inhabiting the continental slope (Relini, 2007). *Galeus melastomus* is a common bycatch species for this fishery – one that is occasionally marketed, but more often discarded at sea due to its low commercial value (Abella and Serena, 2002).

The *S. canicula* specimens were landed and donated by a trawler operating in the port of San Benedetto del Tronto in May 2019. In the Adriatic Sea, bycatch of many cartilaginous fish species also includes *S. canicula*, whose commercial value is not particularly significant.

3.2. Fossil sharks

Six teeth of *Scyliorhinus woodwardi* were collected from the fossiliferous lower Eocene strata of the Ampe quarry at Egem, ca. 40 km west of Ghent, in West-Flanders (Belgium) (Fig. 2). Here, different horizons have long yielded vast amounts of shark and ray teeth (Smith and Smith, 2013). The *S. woodwardi* specimens dealt with herein come from “bed IV” (*sensu* Steurbaut, 1988) of the Egemkapel Clay Member of the Tielt Formation, which is dated to the NP12 Calcareous Nannoplankton Zone,

corresponding to the middle part of the Ypresian (Steurbaud, 1998, 2006). Formed by fossil-rich marine sands, silts and clays, the Tielt Formation reflects deposition in an epicontinental sea of the southern North Sea basin (Smith and Smith, 2013). In particular, “bed IV” consists of lenticular, channeled, fine glauconitic sands featuring abundant elasmobranch teeth, rarer terrestrial vertebrate remains and ubiquitous *Ditrupa* worm-tubes (Smith and Smith, 2013; Reinecke et al., 2024). The depositional setting was located in a shallow coastal marine paleobiotope (Smith and Smith, 2013).

Six teeth of *Pachyscyllium distans* (Probst, 1879) come from Loupian, Hérault (southern France; Fig. 2), where Miocene marine deposits are exposed. These sediments mostly consist of limestones and grey marls that pertain to the Montbazin-Gigean basin, whose sedimentary fill accumulated in-between the Amelias Plateau and Gardiole Mountain, two peri-Mediterranean reliefs made of Mesozoic rocks (Benoit et al., 2011). The Miocene deposits of Hérault are home to an abundant, exceptionally rich elasmobranch assemblage (Cappetta, 1970). The teeth examined in this study were collected in the Péchiney Quarry, specifically from Cappetta’s (1970) “layer 11”. This 25-cm-thick horizon, consisting of lower Middle Miocene (*i.e.*, Langhian) yellowish marls, yields a variety of fossils, including an abundant and exceptionally diverse assemblage of bony and cartilaginous fish teeth as well as fragmentary remains of marine and terrestrial mammals, and macro-invertebrates (Cappetta, 1970). The depositional setting was located in the inner shelf, not far from the coast (Cappetta, 1970).

The twelve Pliocene samples originate from the Baccinello-Cinigiano and Siena-Radicofani basins of Tuscany (central Italy; Fig. 2), which developed in the broad area of the present-day Northern Apennine foothills as the subduction front migrated eastward and the Tyrrhenian Sea formed further west. While the Baccinello-Cinigiano basin was located not far from the present-day coastline, the Siena-Radicofani

Table 2

Recent and fossil shark material (teeth and scales) analyzed in the present paper, referred to geographic location, age, and (for Recent material) to sex, length and maturity.

| CODE | CLASSIFICATION | LOCALITY | AGE | SEX | LENGTH (cm) | MATURITY | TYPE |
|------|---|--|---------------------------------------|--------|----------------|----------|---------------|
| GM1 | <i>Galeus melastomus</i> Rafinesque, 1810 | Porto Savona (Italy) | Recent | female | 45 | 4A | tooth |
| GM3 | <i>Galeus melastomus</i> Rafinesque, 1810 | Porto Savona (Italy) | Recent | female | 28.5 | 1 | tooth |
| GM4 | <i>Galeus melastomus</i> Rafinesque, 1810 | Porto Savona (Italy) | Recent | female | 50 | 3B | tooth |
| GM5 | <i>Galeus melastomus</i> Rafinesque, 1810 | Porto Savona (Italy) | Recent | female | 45 | 2 | tooth |
| GM6 | <i>Galeus melastomus</i> Rafinesque, 1810 | Porto Savona (Italy) | Recent | male | 24 | 1 | tooth |
| GM7 | <i>Galeus melastomus</i> Rafinesque, 1810 | Porto Savona (Italy) | Recent | female | 24 | 1 | tooth |
| GM8 | <i>Galeus melastomus</i> Rafinesque, 1810 | Porto Savona (Italy) | Recent | female | 45.5 | 3B | tooth |
| GM9 | <i>Galeus melastomus</i> Rafinesque, 1810 | Porto Savona (Italy) | Recent | male | 44 | 3 A | tooth |
| GM10 | <i>Galeus melastomus</i> Rafinesque, 1810 | Porto Savona (Italy) | Recent | female | 40 | 1 | tooth |
| GM11 | <i>Galeus melastomus</i> Rafinesque, 1810 | Porto Savona (Italy) | Recent | male | 38.5 | 1 | tooth |
| GM12 | <i>Galeus melastomus</i> Rafinesque, 1810 | Porto Savona (Italy) | Recent | male | 42 | 2 | tooth |
| GM13 | <i>Galeus melastomus</i> Rafinesque, 1810 | Porto Savona (Italy) | Recent | male | 30.5 | 1 | tooth |
| GM14 | <i>Galeus melastomus</i> Rafinesque, 1810 | Porto Savona (Italy) | Recent | female | 24 | 1 | tooth |
| GM16 | <i>Galeus melastomus</i> Rafinesque, 1810 | Porto Santa Margherita Ligure (Italy) | Recent | male | 38 | 1 | tooth |
| GM17 | <i>Galeus melastomus</i> Rafinesque, 1810 | Porto Santa Margherita Ligure (Italy) | Recent | male | 25 | 1 | tooth |
| GM18 | <i>Galeus melastomus</i> Rafinesque, 1810 | Porto Santa Margherita Ligure (Italy) | Recent | female | 26 | 1 | tooth |
| GM19 | <i>Galeus melastomus</i> Rafinesque, 1810 | Porto Savona (Italy) | Recent | male | 28 | 1 | tooth |
| GM20 | <i>Galeus melastomus</i> Rafinesque, 1810 | Porto Savona (Italy) | Recent | female | 26.5 | 1 | tooth |
| GM21 | <i>Galeus melastomus</i> Rafinesque, 1810 | Porto Savona (Italy) | Recent | male | 26 | 1 | tooth |
| SC1 | <i>Scyliorhinus canicula</i> (Linnaeus, 1758) | Porto San Benedetto del Tronto (Italy) | Recent | male | 42 | 3B | scale + tooth |
| SC2 | <i>Scyliorhinus canicula</i> (Linnaeus, 1758) | Porto San Benedetto del Tronto (Italy) | Recent | female | 41 | 2 | scale + tooth |
| SC3 | <i>Scyliorhinus canicula</i> (Linnaeus, 1758) | Porto San Benedetto del Tronto (Italy) | Recent | female | 33 | 2 | scale + tooth |
| SC4 | <i>Scyliorhinus canicula</i> (Linnaeus, 1758) | Porto San Benedetto del Tronto (Italy) | Recent | female | 32 | 2 | scale + tooth |
| SC5 | <i>Scyliorhinus canicula</i> (Linnaeus, 1758) | Porto San Benedetto del Tronto (Italy) | Recent | female | 50 | 3B | scale + tooth |
| SC6 | <i>Scyliorhinus canicula</i> (Linnaeus, 1758) | Porto San Benedetto del Tronto (Italy) | Recent | female | 32 | 3B | scale + tooth |
| SC7 | <i>Scyliorhinus canicula</i> (Linnaeus, 1758) | Porto San Benedetto del Tronto (Italy) | Recent | female | 38 | 3 A | scale + tooth |
| SC8 | <i>Scyliorhinus canicula</i> (Linnaeus, 1758) | Porto San Benedetto del Tronto (Italy) | Recent | female | 36 | 2 | scale + tooth |
| SC9 | <i>Scyliorhinus canicula</i> (Linnaeus, 1758) | Porto San Benedetto del Tronto (Italy) | Recent | female | 32 | 2 | scale + tooth |
| 1 | <i>Scyliorhinus woodwardi</i> (Cappetta, 1976) | Egem, West-Flanders (Belgium) | fossil (lower Eocene, Ypresian, NP12) | – | – | – | tooth |
| 2 | <i>Scyliorhinus woodwardi</i> (Cappetta, 1976) | Egem, West-Flanders (Belgium) | fossil (lower Eocene, Ypresian, NP12) | – | – | – | tooth |
| 3 | <i>Scyliorhinus woodwardi</i> (Cappetta, 1976) | Egem, West-Flanders (Belgium) | fossil (lower Eocene, Ypresian, NP12) | – | – | – | tooth |
| 4 | <i>Scyliorhinus woodwardi</i> (Cappetta, 1976) | Egem, West-Flanders (Belgium) | fossil (lower Eocene, Ypresian, NP12) | – | – | – | tooth |
| 5 | <i>Scyliorhinus woodwardi</i> (Cappetta, 1976) | Egem, West-Flanders (Belgium) | fossil (lower Eocene, Ypresian, NP12) | – | – | – | tooth |
| 6 | <i>Scyliorhinus woodwardi</i> (Cappetta, 1976) | Egem, West-Flanders (Belgium) | fossil (lower Eocene, Ypresian, NP12) | – | – | – | tooth |
| 7 | <i>Pachyscyllium distans</i> (Probst, 1879) | Loupian, Hérault (France) | fossil (Middle Miocene, Langhian) | – | – | – | tooth |
| 8 | <i>Pachyscyllium distans</i> (Probst, 1879) | Loupian, Hérault (France) | fossil (Middle Miocene, Langhian) | – | – | – | tooth |
| 9 | <i>Pachyscyllium distans</i> (Probst, 1879) | Loupian, Hérault (France) | fossil (Middle Miocene, Langhian) | – | – | – | tooth |
| 10 | <i>Pachyscyllium distans</i> (Probst, 1879) | Loupian, Hérault (France) | fossil (Middle Miocene, Langhian) | – | – | – | tooth |
| 11 | <i>Pachyscyllium distans</i> (Probst, 1879) | Loupian, Hérault (France) | fossil (Middle Miocene, Langhian) | – | – | – | tooth |
| 12 | <i>Pachyscyllium distans</i> (Probst, 1879) | Loupian, Hérault (France) | fossil (Middle Miocene, Langhian) | – | – | – | tooth |
| 13 | <i>Pachyscyllium dachiardii</i> (Lawley, 1876) | Rapolano, Tuscany (Italy) | fossil (Pliocene) | – | – | – | tooth |
| 14 | <i>Pachyscyllium dachiardii</i> (Lawley, 1876) | Rapolano, Tuscany (Italy) | fossil (Pliocene) | – | – | – | tooth |
| 15 | <i>Pachyscyllium dachiardii</i> (Lawley, 1876) | Rapolano, Tuscany (Italy) | fossil (Pliocene) | – | – | – | tooth |
| 16 | <i>Pachyscyllium dachiardii</i> (Lawley, 1876) | Rapolano, Tuscany (Italy) | fossil (Pliocene) | – | – | – | tooth |
| 17 | <i>Pachyscyllium dachiardii</i> (Lawley, 1876) | Rapolano, Tuscany (Italy) | fossil (Pliocene) | – | – | – | tooth |
| 18 | <i>Pachyscyllium dachiardii</i> (Lawley, 1876) | Arcille, Tuscany (Italy) | fossil (Pliocene) | – | – | – | tooth |
| 19 | <i>Megascyliorhinus miocaenicus</i> (Antunes and Jonet, 1970) | Arcille, Tuscany (Italy) | fossil (Pliocene) | – | – | – | tooth |

(continued on next page)

Table 2 (continued)

| CODE | CLASSIFICATION | LOCALITY | AGE | SEX | LENGTH (cm) | MATURITY | TYPE |
|------|---|---------------------------|-------------------|-----|----------------|----------|-------|
| 20 | <i>Megascyliorhinus miocaenicus</i> (Antunes and Jonet, 1970) | Arcille, Tuscany (Italy) | fossil (Pliocene) | – | – | – | tooth |
| 21 | <i>Megascyliorhinus miocaenicus</i> (Antunes and Jonet, 1970) | Rapolano, Tuscany (Italy) | fossil (Pliocene) | – | – | – | tooth |
| 22 | <i>Megascyliorhinus miocaenicus</i> (Antunes and Jonet, 1970) | Rapolano, Tuscany (Italy) | fossil (Pliocene) | – | – | – | tooth |
| 23 | <i>Megascyliorhinus miocaenicus</i> (Antunes and Jonet, 1970) | Rapolano, Tuscany (Italy) | fossil (Pliocene) | – | – | – | tooth |
| 24 | <i>Megascyliorhinus miocaenicus</i> (Antunes and Jonet, 1970) | Rapolano, Tuscany (Italy) | fossil (Pliocene) | – | – | – | tooth |

basin is the easternmost of the “central basins” (*sensu* Martini and Sagri, 1993) that accommodated marine deposition along the western side of the Northern Apennines during the late Neogene.

A single tooth of *Pachyscyllium dachiardii* (Lawley, 1876) and two teeth of *Megascyliorhinus miocaenicus* (Antunes and Jonet, 1970) come from the locality of Arcille, in the Baccinello-Cinigiano basin (Fig. 2). Here, Lower Pliocene (*i.e.*, Zanclean) siliciclastics are visible in an inactive quarry, consisting of yellowish sandstones and minor conglomerate layers that are capped by grayish mudstones (Sorbi et al., 2012; Bianucci et al., 2019; Dominici and Forli, 2021). The macrofossil assemblage records a diverse assemblage of marine tetrapods and fishes, including remarkable fossils of sharks and rays (Collareta et al., 2021a, 2021b; Merella et al., 2023). Many of these fossils, comprising those dealt with herein, were collected from a highly productive interval of yellowish sandstones that reflect a shallow-marine, river-influenced setting.

Five teeth of *P. dachiardii* and four teeth of *M. miocaenicus* come from the Siena-Radicofani basin (Fig. 2). These specimens belong in the collection gathered by the late avocational paleontologist Roberto Burroni, which was made at Pliocene outcrops of the Siena-Radicofani basin in the surroundings of Rapolano Terme. Here, the Pliocene is mostly represented by offshore (*i.e.*, outer shelf to upper slope) mudstones where shark teeth are relatively common (Martini and Sandrelli, 2015). Unfortunately, precise geographic and stratigraphic whereabouts are not available for these teeth.

4. Methods

4.1. Extant sample preparation

During landing operations, the specimens were selected and subsequently frozen and stored until the laboratory procedures. For every single specimen, the total length TL (cm), fresh weight (g), sex and ontogenetic stage were recorded following the Data Collection Framework procedure (Follesa and Carbonara, 2019; Mollen, 2019; Table 2). Frozen samples were subsequently transferred to our laboratory. Once the fish were thawed, the mandibles and strips of the skin were hand-sampled by using a scalpel. Pieces were allowed to dry under a fume hood (turned off to avoid scattering the samples, which, being very light, were at risk of flying away) for about ten days. At this point, teeth and scales were further extracted under a stereomicroscope by using a stick with a needle mounted at the tip.

Three to four teeth for each specimen of *Galeus melastomus* (19 specimens, 58 teeth) and three teeth + three scales for each specimen of *Scyliorhinus canicula* (9 specimens, 27 teeth and 27 scales) were prepared, adding up to 112 samples, including 85 teeth and 27 scales. Before measurements (see below), each sample was thoroughly washed with ultrapure Millipore water. However, it should be noted that any micro-residues do not affect the diffractometric measurements and are then removed by a laser pre-ablation step before the spectrometric measurements.

4.2. Sample mounting

Recent and fossil specimens were mounted on aluminium stubs previously covered with carbon-conductive adhesive tape to perform the μ -XRD analysis. Specimens selected for the LA-ICPMS analyses were aligned onto glass slides covered with tape to facilitate the sample arrangement and data collection. Whenever possible, signals were detected from both the crown and the root of each tooth (Fig. 1). Scales were analyzed focusing on the enameloid part of the samples.

4.3. Sample imaging

Electron microscopy data of Recent (Figs. 3–4) and fossil (Fig. 5) materials were collected using the Scanning Electron Microscope (SEM) JEOL JSM–6010PLUS/LA InTouchScope at the Department of Chemical and Geological Sciences, University of Modena and Reggio Emilia, Modena, Italy. Scanning Electron Microscope measurements were performed in high vacuum with an accelerating voltage between 5 and 20 keV. Larger fossil specimens (Fig. 5) were photographed using led macro ring flash, a Pentax K1 digital camera equipped with a macro 90 mm f/2.8 1:1 and a led macro ring flash.

4.4. X-ray microdiffraction (μ -XRD)

X-ray microdiffraction is a powerful, non-destructive tool for obtaining crystallographic information when dealing with small-sized samples. This technique involves the collimation of X-rays to form a small beam (up to 10 μ m in diameter) before irradiating a sample, thus allowing for the study of some structural properties of minerals such as unit cell parameters, the degree of crystallinity, the size of crystallites and their preferential orientations, and the mineralogical composition of the crystalline phases (Medici et al., 2020). Measurements were performed at the Institute of Methodologies for Environmental Analysis of the National Research Council of Italy, Tito Scalo (Potenza, Italy). Data were acquired using a Rigaku D/MAX RAPID diffraction system operating at 40 kV and 30 mA, equipped with a CuK α source, a curved-image-plate detector, a flat graphite monochromator, a variety of beam collimators, a motorized stage and a microscope for the accurate positioning of the samples. Measurements were performed in reflection mode using a 300- μ m collimator (collection times of 10, 12 and 13 min) and a 100- μ m collimator (collection time of 60 min) by varying the Omega and Phi angles between one sample and the other to fit with the instrument geometry, thus obtaining a significant number of diffraction effects with a maximized signal-to-noise ratio. The μ -XRD data were collected as two-dimensional images and then converted into I-2 θ profiles using the Rigaku R-AXIS Display software.

The 300- μ m collimator proved suitable to obtain accurate values of bioapatite cell parameters for both the crowns and roots of the fossil specimens. The same 300- μ m collimator was also used to analyze the tooth crown and scales (enameloid) of the extant sharks as well as some tooth roots of the same specimens. The 100- μ m collimator was used to refine the results obtained from some smaller samples. After

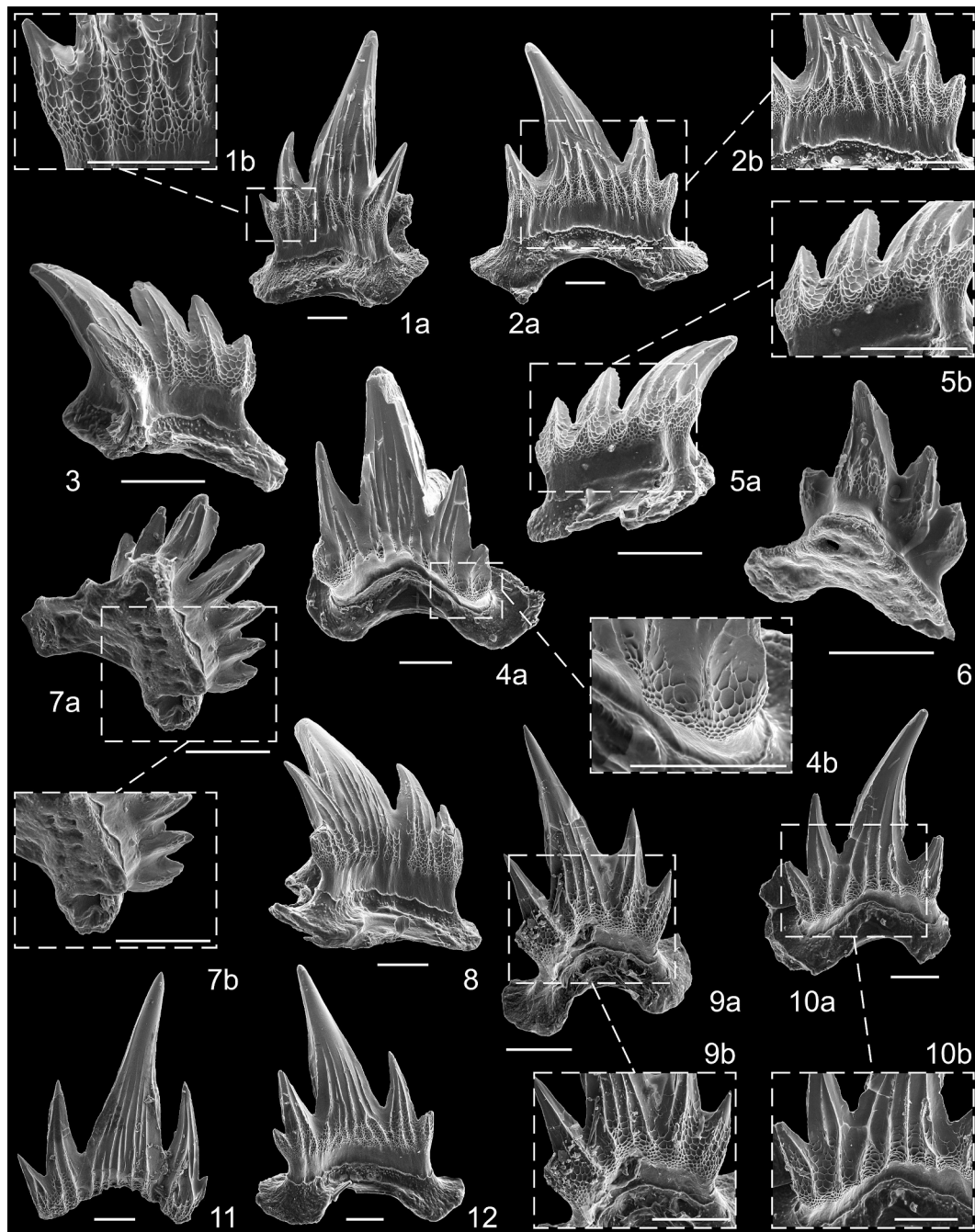


Fig. 3. Recent specimens of *Galeus melastomus* Rafinesque, 1810 analyzed in this study. 1a-b, IPUM 35224; tooth of specimen 4A. Porto Savona, Italy. 2a-b, IPUM 35225; tooth of specimen 4B. Porto Savona, Italy. 3, IPUM 35226; tooth of specimen 20A. Porto Savona, Italy. 4a-b, IPUM 35227; tooth of specimen 5A. Porto Savona, Italy. 5a-b, IPUM 35228; tooth of specimen 14C. Porto Savona, Italy. 6, IPUM 35229; tooth of specimen 6B. Porto Savona, Italy. 7a-b, IPUM 35230; tooth of specimen 7A. Porto Savona, Italy. 8, IPUM 35231; tooth of specimen 16A. Porto Santa Margherita Ligure, Italy. 9a-b, IPUM 35232; tooth of specimen 20B. Porto Savona, Italy. 10a-b, IPUM 35233; tooth of specimen 12C. Porto Savona, Italy. 11, IPUM 35234; tooth of specimen 9B. Porto Savona, Italy. 12, IPUM 35235; tooth of specimen 8A. Porto Savona, Italy. Scale bars correspond to 200 μm .

measurements, the unit-cell parameters (a , c and the cell volume) were refined using UnitCell software (Holland and Redfern, 1997). From these X-ray diffraction measurements, it was also possible to obtain two independent evaluations of the crystallinity of the studied samples. The first procedure consisted in calculating the Crystallinity Index (CI) according to Person et al. (1995). Another different procedure used Full Width at Half Maximum (FWHM) of the (300) and (002) reflections by applying the Scherrer equation to calculate the width along the a axis and length along the c axis of crystallites, respectively (Dumont et al., 2011). An estimation of the number of unit cells per crystallite along the

a and c axes was obtained by calculating the width/ a and length/ c ratios.

4.5. REE measurement

Trace element concentrations were determined using a Thermo Fisher Scientific ICP-MS X Series II, equipped with a 213 nm laser ablation device (UP-213) from New Wave Research at the Centro Interdipartimentale Grandi Strumenti (CIGS) of the University of Modena and Reggio Emilia, Italy. Prior to optimizing the laser ablation for the phosphatic matrix, the

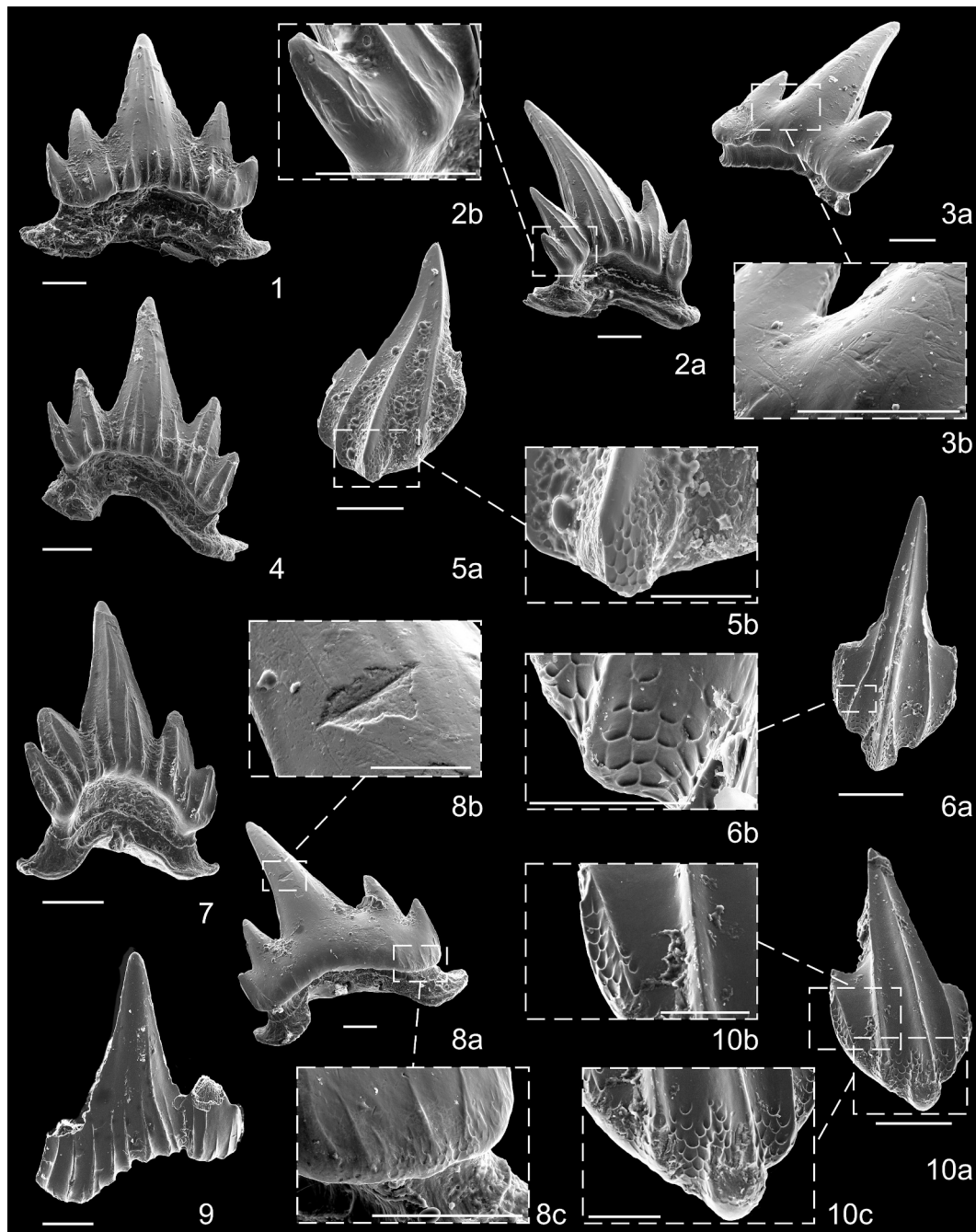


Fig. 4. Recent specimens of *Scyliorhinus canicula* (Linnaeus, 1758) analyzed in this study. 1, IPUM 35236; tooth of specimen 7A. Porto San Benedetto del Tronto, Italy. 2a-b, IPUM 35237; tooth of specimen 8E. Porto San Benedetto del Tronto, Italy. 3a-b, IPUM 35238; tooth of specimen 8D. Porto San Benedetto del Tronto, Italy. 4, IPUM 35239; tooth of specimen 6B. Porto San Benedetto del Tronto, Italy. 5a-b, IPUM 35240; scale of specimen 8A. Porto San Benedetto del Tronto, Italy. 6a-b, IPUM 35241; scale of specimen 2A. Porto San Benedetto del Tronto, Italy. 7, IPUM 35242; tooth of specimen 2C. Porto San Benedetto del Tronto, Italy. 8a-c, IPUM 35243; tooth of specimen 5B. Porto San Benedetto del Tronto, Italy. 9, IPUM 35244; tooth of specimen 1A. Porto San Benedetto del Tronto, Italy. 10a-c, IPUM 35245; scale of specimen 2B. Porto San Benedetto del Tronto, Italy. Scale bars correspond to 200 μm (except for 5b, 8b, 10b and 10c: 100 μm).

instrument was tuned using the NIST 610 and NIST 612 glasses to measure the intensity of the U and Th signals (U/Th vs U) under optimal working conditions. Specifically, the abundance ratios between the two standard glasses were assessed to verify the accuracy of the mass measurements.

As the calibration of ablation parameters is highly matrix-dependent and crucial for obtaining results comparable with literature data, a calibration strategy employing both silica and phosphatic standards was utilized. The employed approach substantially parallels those described in previous work (Nardelli et al., 2016; Ferretti et al., 2017, 2023; Malferrari et al., 2019, 2024; Medici et al., 2021). In brief, after tuning

the instrument as described above, a tablet was prepared with the NIST 1400 (bone ash) standard and, using NIST SRM 610 and NIST SRM 612 as calibration standards, the ablation parameters were adjusted until the concentrations of selected trace elements in the NIST 1400 tablet closely matched the certified values. The optimized ablation parameters were then applied to the standards (NIST SRM 610 and NIST SRM 612) as well as to the samples. To prepare the sample surfaces, a pre-ablation protocol was applied, involving mild ablation at about 1/10 of the operating fluence conditions; this procedure allows any surface contaminants to be removed before measurement. The parameters for pre-ablation were as

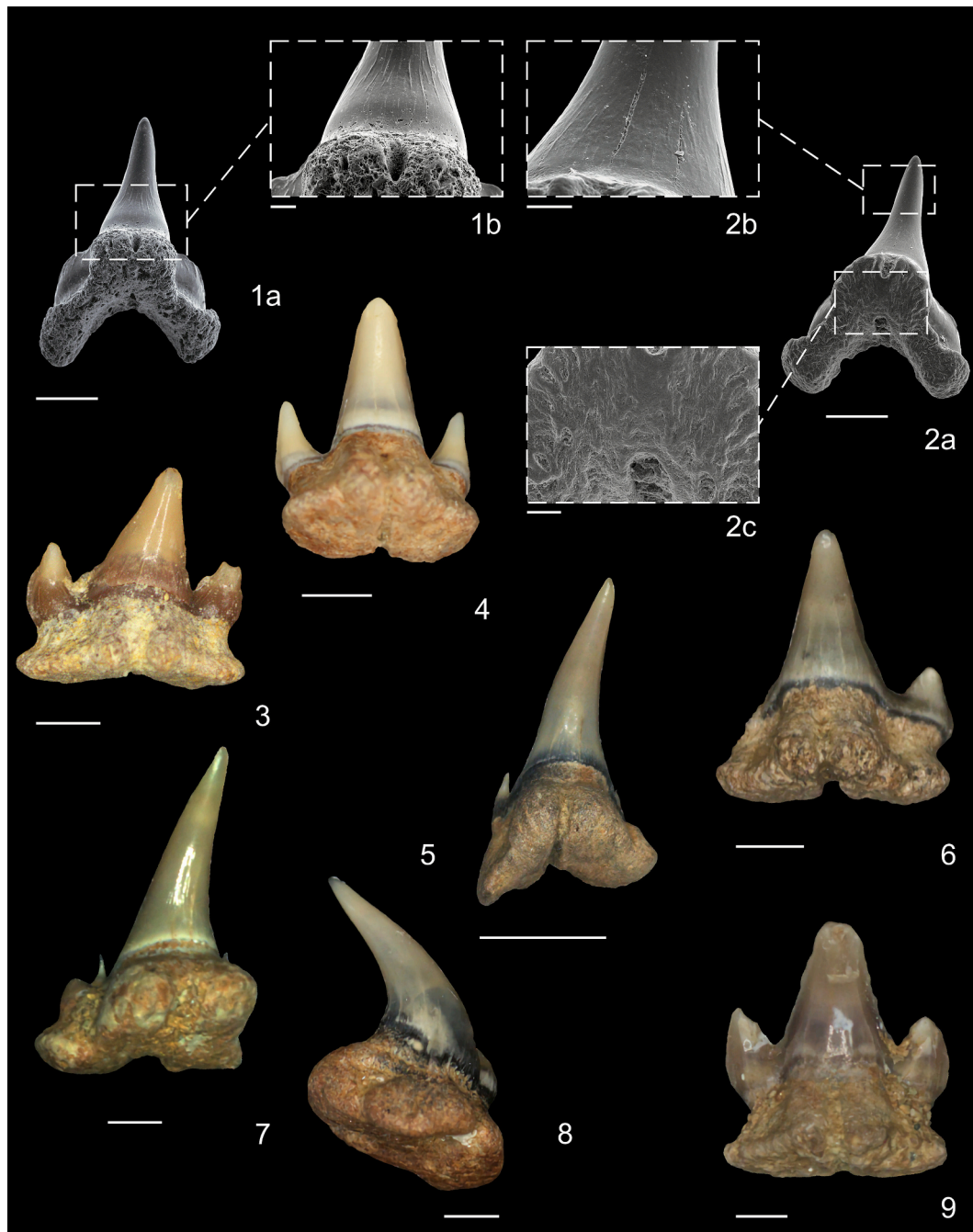


Fig. 5. Fossil specimens belonging to the family Scyliorhinidae analyzed in this study. 1–2, ERB NN 001 and ERB NN 002, *Scyliorhinus woodwardi* Cappetta, 1976; specimens 5 and 1, respectively, with details in the insets 1b, 2b and 2c. Lower Eocene (Ypresian), Egem, northwestern Belgium. Scale bars: 500 μm for 1a and 2a, 100 μm for 1, 2b and 2c. 3, ERB NN 007, *Pachyscyllium distans* (Probst, 1879); specimen 10, Middle Miocene (Langhian), Loupian, southern France. Scale bar: 1 mm. 4, 6, GAMPS NN 001 and GAMPS NN 002, *Pachyscyllium dachtiardii* (Lawley, 1876); specimens 15 and 17, respectively. Pliocene, Rapolano, central Italy. Scale bars: 1 mm. 5, 8, GAMPS NN 007 and GAMPS NN 008, *Megascyliorhinus miocaenicus* (Antunes and Jonet, 1970); specimens 24 and 21, respectively. Pliocene, Rapolano, central Italy. Scale bars: 5 mm (5) and 1 mm (8). 7, GAMPS NN 009, *Megascyliorhinus miocaenicus* (Antunes and Jonet, 1970); specimen 20. Pliocene, Arcille, central Italy. Scale bar: 1 mm. 9, GAMPS NN 003, *Pachyscyllium dachtiardii* (Lawley, 1876); specimen 18. Pliocene, Arcille, central Italy. Scale bar: 1 mm.

follows: 65 μm spot size, 30% energy intensity, 10 Hz frequency, 5 seconds of dwell time, and a helium flux of 600 ml/min as carrying gas. After, the samples were ablated with 55 μm spots. The laser beam operated at a fluence between 8.5 and 9.5 J/cm^2 (80% energy intensity) and a frequency of 10 Hz for 45 seconds at each spot. Each sample was analyzed using at least three spots positioned in a closed area.

The following isotopes were measured: ^{24}Mg , ^{27}Al , ^{39}K , ^{48}Ti , ^{55}Mn , ^{57}Fe , ^{88}Sr , ^{89}Y , ^{138}Ba , ^{139}La , ^{140}Ce , ^{141}Pr , ^{146}Nd , ^{147}Sm , ^{153}Eu , ^{157}Gd , ^{159}Tb , ^{163}Dy , ^{165}Ho , ^{166}Er , ^{169}Tm , ^{172}Yb , ^{175}Lu , ^{178}Hf , ^{208}Pb , ^{232}Th and

^{238}U . Calcium was used as an internal standard assuming a concentration of 39.5 wt%. The repeatability of the LA-ICP-MS measurements, expressed as relative standard deviation (RSD), was approximately 5%, based on analyses of the NIST SRM 612 glass. Analytical precision for the tooth samples typically ranged between 5 and 20%, depending on sample inhomogeneities as well as on the concentration of the analytes. The quality control reference material NIST 1400, prepared as pressed tablet, was also measured during the session.

Each point represented in the diagrams that will be discussed below

is the average of at least three measurements (outliers have been removed). The error is not reported but falls within the size of the symbol.

4.6. Repository

The Recent analyzed materials are housed in the Paleontological Collections (= IPUM) of the Department of Chemical and Geological Sciences, University of Modena and Reggio Emilia, Modena, Italy (accession numbers IPUM 35224 to IPUM 35245). The fossil materials are housed at the Elasmobranch Research Belgium (= ERB), Bonheiden, Belgium and at GAMPs Geopaleontological Museum, Scandicci, Italy, with specimen numbers ERB NN (= not numbered) 001 to ERB NN 012 (for the Eocene and Miocene specimens) and GAMPs NN 001 to GAMPs NN 012 (for the Pliocene specimens), respectively.

5. Results

5.1. X-ray microdiffraction

X-ray microdiffraction revealed that extant and fossil shark teeth bear different bioapatite cell parameters and crystallinity indices. The excellent macroscopic preservation of the fossil materials, consisting of largely complete teeth, and their low content of organic matter allowed for the systematic collection of signals from both the crowns and roots. The same was not always possible in samples from extant sharks due to a greater abundance of organic matter, which decreases the crystallinity of the bioapatite lattice of dentine. Nevertheless, no chemical treatment to remove organic matter was applied, as such procedures are highly sample-dependent and may alter the crystallinity of bioapatite, potentially affecting the reliability of X-ray diffraction measurements and introducing bias into comparisons between extant and fossil specimens.

Comparisons between groups are expressed by value ranges, averages (numbers in parentheses indicate the standard deviation of mean values), and Student *t*-test *p*-values. Significance levels are $\alpha = 0.01$ to highlight the diverse response of two groups and $\alpha = 0.05$ to underline the lack of meaningful differences between them.

The *c* vs *a* parameters for the studied bioapatite samples are plotted in Fig. 6. In fossil teeth, the cell parameter *a* revealed significantly higher values for crowns ($a = 9.360 \div 9.387 \text{ \AA}$, $\bar{a} = 9.374(7) \text{ \AA}$) than for roots ($a = 9.309 \div 9.369 \text{ \AA}$, $\bar{a} = 9.337(15) \text{ \AA}$), as confirmed by the Student *t*-test, with a *p*-value < 0.01. The greater variability observed in the tooth roots is likely due to diagenesis, as roots are originally richer in organic matter than crowns; this is further supported by the high standard deviations of the averages. Analyses of the *c* cell parameter confirm the differences (*p*-value < 0.01 of the Student *t*-test) between the crowns ($c = 6.860 \div 6.887 \text{ \AA}$, $\bar{c} = 6.878(6) \text{ \AA}$) and roots ($c = 6.879 \div 6.906 \text{ \AA}$, $\bar{c} = 6.887(6) \text{ \AA}$) of fossil teeth. Unlike the *a* parameter, the *c* parameter exhibits no substantial differences in standard deviations. Moreover, a slight inverse correlation between *c* and *a* is highlighted (Pearson correlation coefficient $R = -0.74$).

Extant shark crowns exhibit higher values for both the *a* parameter and cell volume compared to all the fossil elements; this suggests that carbon is present in the crown of fossil teeth, although to a lesser extent than in the roots. A synthesis of the unit cell parameters of the crowns of extant sharks is $a = 9.381 \div 9.420 \text{ \AA}$, $\bar{a} = 9.400(7) \text{ \AA}$; $c = 6.866 \div 6.893 \text{ \AA}$, $\bar{c} = 6.882(5) \text{ \AA}$; $V = 524.3 \div 528.7 \text{ \AA}^3$, $\bar{V} = 526.6(8) \text{ \AA}^3$. A key finding of the tooth root analyses is the range of crystallographic parameters: $a = 9.360 \div 9.419 \text{ \AA}$, $\bar{a} = 9.399(17) \text{ \AA}$; $c = 6.857 \div 6.893 \text{ \AA}$, $\bar{c} = 6.874(10) \text{ \AA}$; $V = 520.9 \div 527.9 \text{ \AA}^3$, $\bar{V} = 525.9(2.1) \text{ \AA}^3$; due to the presence of organic matter, the samples exhibit low crystallinity, which limits the accuracy of the measured data.

The unit cell parameters measured for the scales of extant sharks show no significant differences compared to the values obtained for the extant crowns. The mean parameters are: $a = 9.392 \div 9.409 \text{ \AA}$, $\bar{a} =$

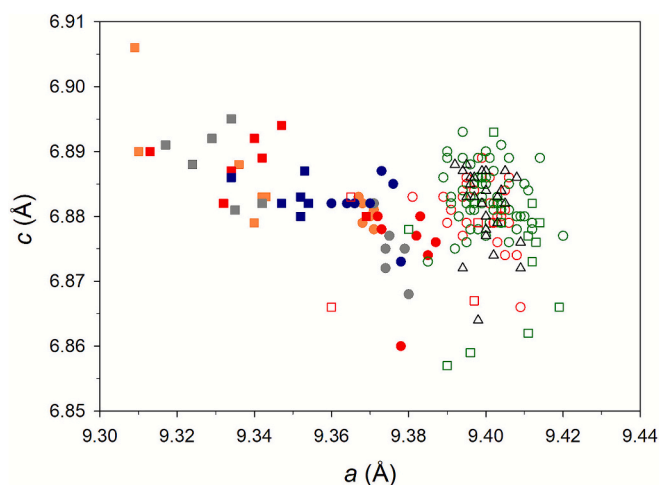


Fig. 6. Scatter plot of cell parameter *c* vs *a* of Recent and fossil shark teeth and Recent scales. Filled and open symbols identify fossil and Recent samples, respectively. In fossil samples measurements were taken both on crown (circles) and root (squares). Colour: orange, *Scyliorhinus woodwardi*; grey, *Pachyscyllium distans*; filled red, *Pachyscyllium dachardii*; filled dark blue, *Megascyliorhinus miocaenicus*; open red, *Scyliorhinus canicula*; open green, *Galeus melastomus*; triangle, *Scyliorhinus canicula* scales. (For interpretation of the references to colour in this figure legend, the reader is referred to the web version of this article.)

$9.400(5) \text{ \AA}$; $c = 6.864 \div 6.888 \text{ \AA}$, $\bar{c} = 6.882(6) \text{ \AA}$; $V = 525.1 \div 527.8 \text{ \AA}^3$, $\bar{V} = 526.6(6) \text{ \AA}^3$. This lack of difference is statistically confirmed by the *p*-value > 0.05 of the Student *t*-test applied to the *a* and *c* parameters as well as to the unit cell volumes.

The relationship between the crystallinity index CI (Person et al., 1995) vs the cell volumes of the studied samples is illustrated in Fig. 7. Fossil sharks show roots with lower CI values ($CI = 0.094 \div 0.545$, $\bar{CI} = 0.263(114)$) and lower unit cell volumes ($V = 517.1 \div 523.0 \text{ \AA}^3$, $\bar{V} = 519.9(1.4) \text{ \AA}^3$) compared to the corresponding crowns ($CI = 0.682 \div 1.280$, $\bar{CI} = 0.825(133)$; $V = 522.1 \div 524.8 \text{ \AA}^3$, $\bar{V} = 523.4(7) \text{ \AA}^3$); these trends are confirmed by a *p*-value < 0.01 of the Student *t*-test applied to both the CI and cell volumes. Crystallinity indices of the crowns of extant sharks are characterized by a high variability ($CI = 0.126 \div 1.681$, $\bar{CI} = 0.864(307)$); anyway, they are still comparable with the crowns of fossil samples ($\bar{CI} = 0.825(133)$) as confirmed by the *p*-value > 0.05 of the Student *t*-test. The reduced diagenesis affecting the

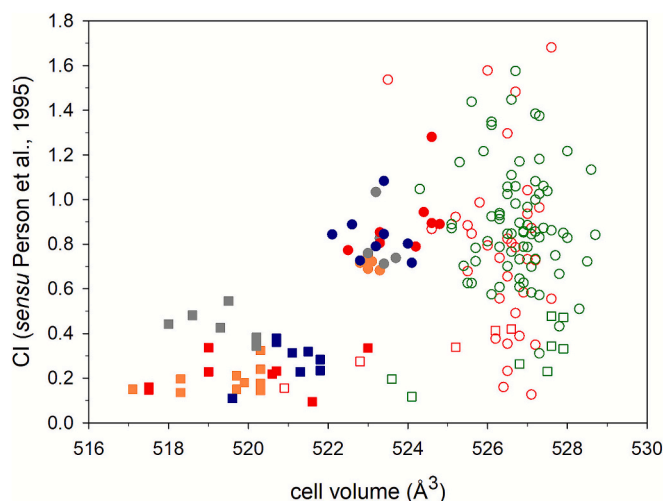


Fig. 7. Scatter plot of CI, according to Person et al. (1995), vs the cell of Recent and fossil shark teeth. Legend like in Fig. 6.

fossil tooth crowns seems to have preserved a crystallinity similar to that of extant shark teeth. As will be highlighted in the Discussion, this suggests that while the incorporation of carbon into the fossil crowns is likely responsible for decreasing the unit cell volumes, it does not modify the overall crystallinity. The following results introduce an alternative method for crystallinity evaluation that may help resolve this open question.

The numbers of unit cells of crystallites along the crystallographic a and c axes (respectively $N_{\text{UnitCell}(a)}$ and $N_{\text{UnitCell}(c)}$) are plotted in Fig. 8; these values correspond to the width and length of crystallites (Fig. SM-1) normalized according to their a and c parameters. The tooth parameters of the extant *G. melastomus* and *S. canicula* utilize the same symbols to enhance the visual clarity across both figures.

The fossil shark samples have roots characterized by lower width and length values ($\text{width} = 18 \div 53$ nm, $\overline{\text{width}} = 34(9)$ nm, $N_{\text{UnitCell}(a)} = 19 \div 57$, $\overline{N_{\text{UnitCell}(a)}} = 37(10)$; $\text{length} = 40 \div 74$ nm, $\overline{\text{length}} = 53(8)$ nm, $N_{\text{UnitCell}(c)} = 58 \div 107$, $\overline{N_{\text{UnitCell}(c)}} = 77(12)$) with respect to the corresponding crowns ($\text{width} = 69 \div 90$ nm, $\overline{\text{width}} = 76(5)$ nm, $N_{\text{UnitCell}(a)} = 74 \div 96$, $\overline{N_{\text{UnitCell}(a)}} = 81(6)$; $\text{length} = 60 \div 128$ nm, $\overline{\text{length}} = 84(17)$ nm, $N_{\text{UnitCell}(c)} = 87 \div 185$, $\overline{N_{\text{UnitCell}(c)}} = 122(24)$); these trends are confirmed by the p -value < 0.01 of the Student t -test applied to the width and length values. Roots exhibit higher $N_{\text{UnitCell}(c)}$ values than $N_{\text{UnitCell}(a)}$ values, as highlighted by the bisector line in Fig. 8 and confirmed by the p -value < 0.01 of the Student t -test applied to length and width values. Conversely, the width and length values of the crowns are more randomly distributed; this is evidenced by the high standard deviations for length and $N_{\text{UnitCell}(c)}$ values, which are probably related to preferential crystal orientations characterizing the crowns. The Student t -test revealed substantial uncertainty regarding the trends of width and length; while the test showed $\overline{\text{length}} > \overline{\text{width}}$ with p -value < 0.05 but > 0.01 , it attested a clear difference for $\overline{N_{\text{UnitCell}(c)}} > \overline{N_{\text{UnitCell}(a)}}$ with a p -value < 0.01 . This discrepancy is attributed to the values of the unit cell parameters $a > c$. These findings are further corroborated by data on the extant sharks, which do not exhibit well-defined trends for crowns, as confirmed by the p -value < 0.01 of the Student t -test. Lower $N_{\text{UnitCell}(a)}$ than $N_{\text{UnitCell}(c)}$ values ($N_{\text{UnitCell}(a)}$

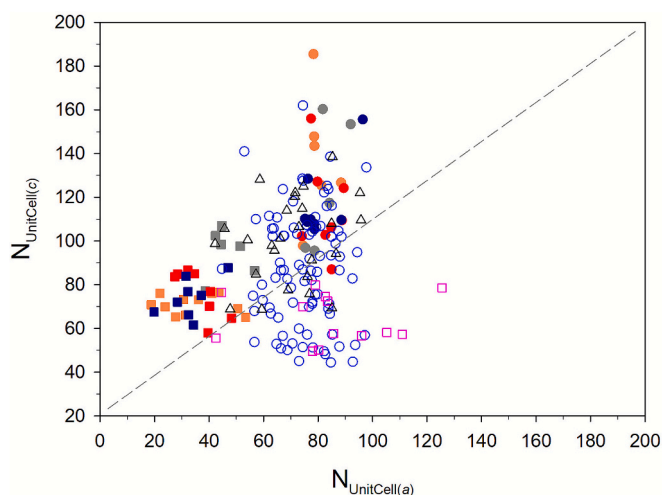


Fig. 8. Scatter plot of the numbers of unit cells of crystallites along the a and c axes of Recent and fossil shark teeth. Filled and open symbols identify fossil and Recent samples, respectively. Measurements were taken both on crown (circles) and root (squares). Colour: orange, *Scyliorhinus woodwardi*; grey, *Pachyscyllium distans*; filled red, *Pachyscyllium dachardii*; filled dark blue, *Megascyliorhinus mioceanicus*; open pink square, *Scyliorhinus canicula* and *Galeus melastomus* roots; open blue circles, *Scyliorhinus canicula* and *Galeus melastomus* crown; triangle, *Scyliorhinus canicula* scales. (For interpretation of the references to colour in this figure legend, the reader is referred to the web version of this article.)

$(a) = 45 \div 98$, $\overline{N_{\text{UnitCell}(a)}} = 75(11)$; $N_{\text{UnitCell}(c)} = 44 \div 162$, $\overline{N_{\text{UnitCell}(c)}} = 87(26)$) contrast with width $>$ length values ($\text{width} = 42 \div 92$ nm, $\overline{\text{width}} = 71(10)$ nm; $\text{length} = 31 \div 112$ nm, $\overline{\text{length}} = 60(18)$ nm). The greater number of unit cells along the c axis compared to the a axis is not enough to form crystallites with $\text{length} > \text{width}$.

The comparison between the crystallinities of extant and fossil crowns can be further refined by analyzing parameters such as width, length, $N_{\text{UnitCell}(a)}$ and $N_{\text{UnitCell}(c)}$, especially following the observed lack of differences found by CI values. Statistical analyses indicate that fossil crowns reveal slightly higher crystallinity than extant shark crowns. This difference is highlighted by variations in the average values (Student t -test, p -values < 0.01): $76(5)_{\text{fossil}} > 71(10)_{\text{extant}}$ (width), $84(17)_{\text{fossil}} > 60(18)_{\text{extant}}$ (length), $81(6)_{\text{fossil}} > 75(11)_{\text{extant}}$ ($N_{\text{UnitCell}(a)}$), $122(24)_{\text{fossil}} > 87(26)_{\text{extant}}$ ($N_{\text{UnitCell}(c)}$). Thus, the incorporation of carbon into the apatite lattice of the fossil crowns influences and enhances the crystallinity of the biominerals.

The presence of organic matter in the roots of the extant sharks complicated the analysis, resulting in high standard deviations and, consequently, reduced significance for these tooth parts. The measured parameters are: $\text{width} = 40 \div 118$ nm, $\overline{\text{width}} = 79(22)$ nm, $N_{\text{UnitCell}(a)} = 43 \div 126$, $\overline{N_{\text{UnitCell}(a)}} = 84(23)$; $\text{length} = 34 \div 55$ nm, $\overline{\text{length}} = 44(8)$ nm, $N_{\text{UnitCell}(c)} = 50 \div 80$, $\overline{N_{\text{UnitCell}(c)}} = 64(11)$. According to the Student t -test, width is greater than length (p -value < 0.01), whereas $N_{\text{UnitCell}(a)} > N_{\text{UnitCell}(c)}$ is greater only for p -value < 0.05 . Moreover, both length and $N_{\text{UnitCell}(c)}$ are lower than the values obtained for the corresponding crowns (p -value < 0.01). However, the limited significance of these data must be acknowledged due to the high organic matter content.

The results obtained for the scales of the extant sharks do not show significant differences between width and length (p -value = 0.36 of Student t -test) as they exhibit $N_{\text{UnitCell}(c)} > N_{\text{UnitCell}(a)}$ ($\text{width} = 40 \div 90$ nm, $\overline{\text{width}} = 66(13)$ nm, $N_{\text{UnitCell}(a)} = 42 \div 96$, $\overline{N_{\text{UnitCell}(a)}} = 70(14)$; $\text{length} = 47 \div 95$ nm, $\overline{\text{length}} = 69(13)$ nm, $N_{\text{UnitCell}(c)} = 69 \div 138$, $\overline{N_{\text{UnitCell}(c)}} = 101(20)$). Unlike teeth, scales form crystallites with more even dimensions (both width and length). The values of width and $N_{\text{UnitCell}(a)}$ do not reveal differences compared to the crystallites comprising the crowns of extant sharks, whereas differences exist between the corresponding length and $N_{\text{UnitCell}(c)}$ values (p -value < 0.01). In particular, the length of the crown crystallites is smaller compared to that of the crystallites of scales. In general, the width, length, $N_{\text{UnitCell}(a)}$, and $N_{\text{UnitCell}(c)}$ values of scales are lower than the corresponding values of fossil crowns (Student t -test, p -value < 0.01).

5.2. Rare Earth Element signature

As pointed out earlier, the preservation of the fossil teeth has allowed to collect signals from both the crowns and roots; in turn, the same was not always possible with extant samples since they are often characterized by target element concentrations below the detection limit. Both fossil crowns and roots are characterized by a substantial enrichment of MREE and HREE as evidenced by the linear distribution of normalized Y vs normalized La, Gd and Yb (Fig. 9), which are assumed as representative of LREE, MREE and HREE, respectively. Similarly, a direct correlation exists between the normalized values of Pr, Gd and Yb vs La (Fig. SM-2). As will be detailed in the Discussion, these trends denote the effect of diagenesis regardless of age, as confirmed by the linear correlations between Y and the sums of light (ΣLREE), middle (ΣMREE) and heavy (ΣHREE) REE (Fig. 10). The better correlation (higher R^2) between Y and ΣHREE (Fig. 10c) compared to ΣLREE and ΣMREE (Fig. 10b-c) confirms that a diagenetic signature is present in all the fossil samples.

The Ce/Ce^* vs Pr/Pr^* diagram (Fig. 11) reveals the grouping of different samples according to their geological age only, i.e., crowns and roots with the same age cluster accordingly. This denotes markedly different redox conditions in the settings that yielded the fossils,

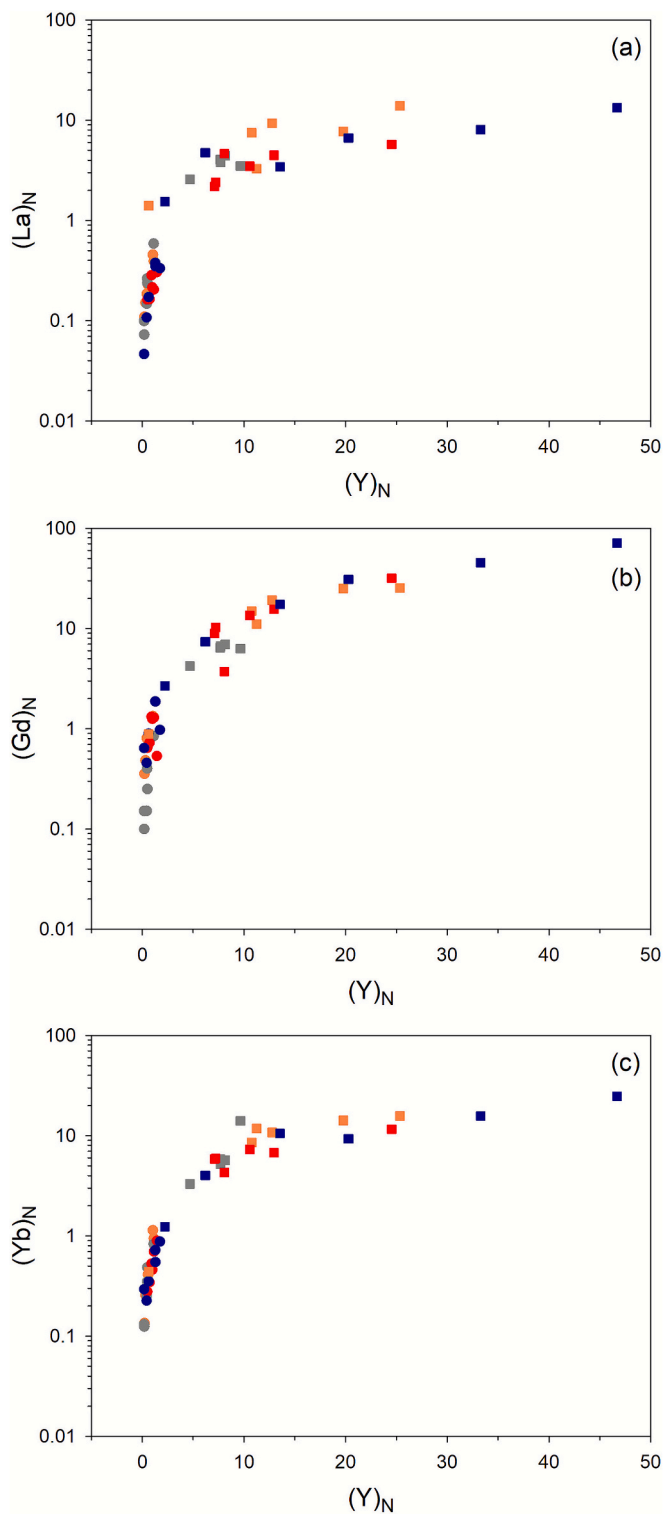


Fig. 9. Crossplots of the normalized (McLennan, 2001) concentration of La (a), Gd (b) and Yb (c) vs Y of fossil shark teeth. Circles and squares identify measurements on crown and root, respectively. Colour: orange, *Scyliorhinus woodwardi*; grey, *Pachyscyllium distans*; red, *Pachyscyllium dachiardii*; dark blue, *Megascyliorhinus miocaenicus*. (For interpretation of the references to colour in this figure legend, the reader is referred to the web version of this article.)

although none of them exhibit major anomalies.

In extant sharks, the direct correlations (better evident in *G. melastomus* than in *S. canicula*) that can be observed between e.g., Σ REE and Σ HREE vs Y, Σ REE vs Th, U vs Th, (Pr)_n vs (La)_n and (Gd)_n vs

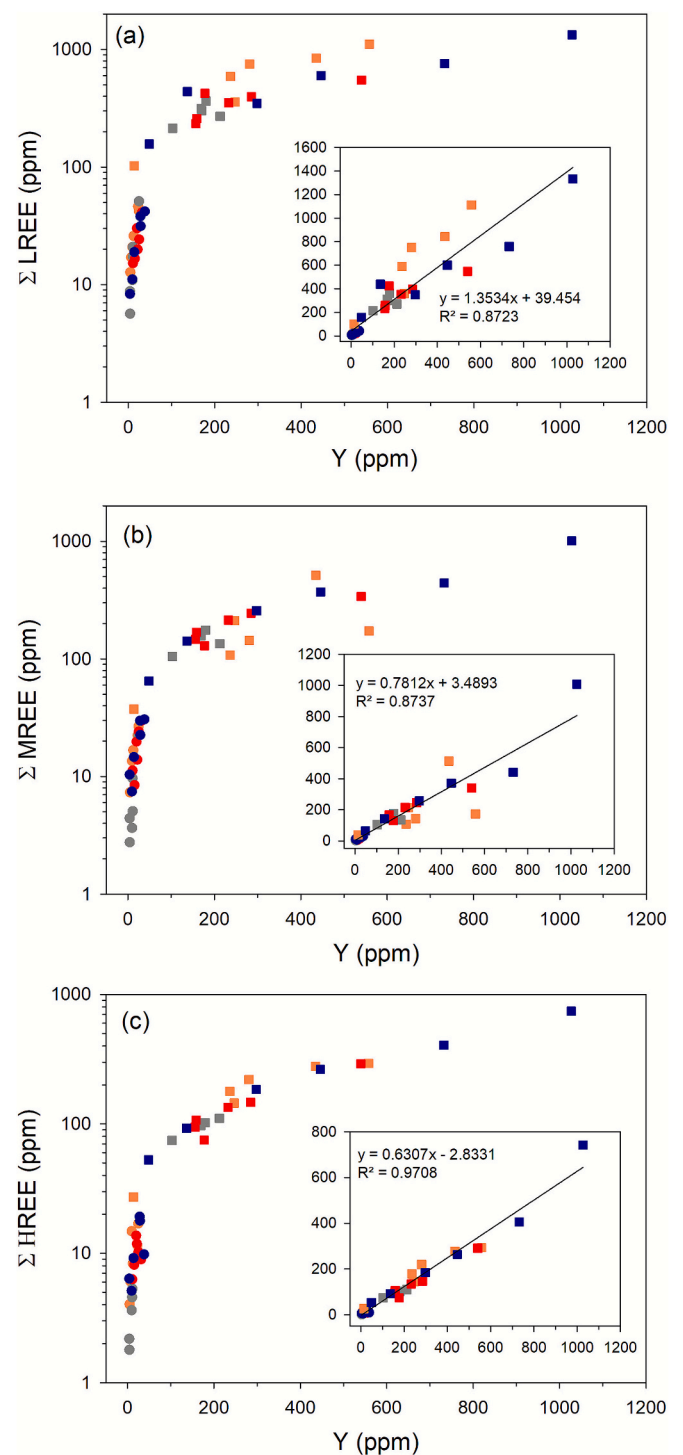


Fig. 10. Linear correlations between Y and sum of light (Σ LREE) (a), middle (Σ MREE) (b) and heavy (Σ HREE) (c) REE. For a clearer demonstration of the linear correlation, the y-axis is plotted on both a logarithmic scale (left) and a linear scale (right). The lines are the linear regression plots (equations and R² are reported on each plot). Symbols correspond to those shown in Fig. 9.

(La)_n (Fig. 12) suggest that all the chemical elements analyzed herein had the same source. A weak positive anomaly of Ce and La (Fig. 13), evident only in *G. melastomus*, may arise from a combination of local environmental conditions, biological preferences and/or other biogeochemical factors. The greater dispersion of the data and the poor correlations found in *S. canicula* are possibly due to their extremely low REE contents, which may affect the data accuracy.

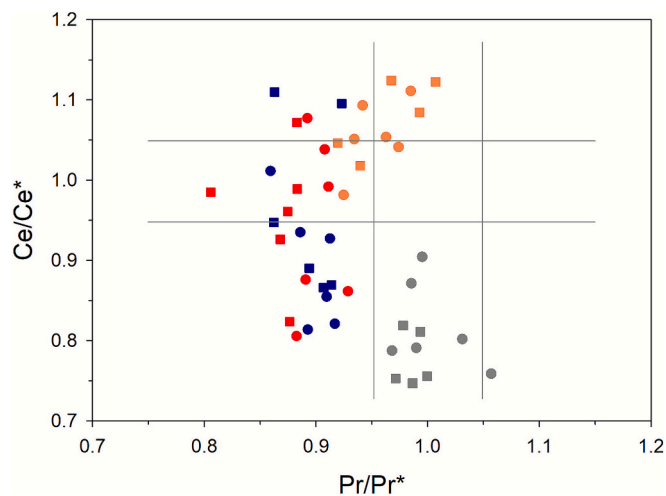


Fig. 11. Location of the fossil samples in the McLennan (2001) normalized plots of (Ce/Ce^*) vs (Pr/Pr^*) . Adapted from Kowal-Linka et al. (2014). Symbols correspond to those shown in Fig. 9.

6. Discussion

The crystallographic and geochemical patterns observed in this study provide new insights into the transformations of bioapatite and their implications for shark functional morphology and paleoenvironmental reconstructions. The systematic reduction of the a lattice parameter and unit cell volume in fossils, together with the increase of the c parameter and crystallinity (Fig. 6), can be interpreted as the outcome of organic matter loss and subsequent incorporation of carbon into the bioapatite lattice (Senter, 2022). This interpretation is consistent with previous work showing that carbonate substitution reduces a values while slightly increasing c (Cacciotti, 2016).

The comparison between crowns and roots highlights the strong influence of original tissue composition on diagenetic outcomes. Fossil crowns consistently retain higher crystallinity and unit cell volumes compared to roots (Fig. 7), reflecting their lower organic content in life and reduced susceptibility to carbon incorporation. By contrast, roots, originally richer in organic matter, underwent stronger alteration, showing decreased volumes and lower crystallinity. These differences are statistically significant, emphasizing that root is especially vulnerable to modification. The REE results reinforce this biological–diagenetic interplay. Fossil samples exhibit strong correlations between Y and ΣREE , ΣMREE , and ΣHREE (Fig. 10). This confirms that their chemical signatures were controlled by diagenetic uptake rather than by the primary seawater composition, a finding consistent with studied on other organisms (Lécuyer et al., 2004; Chen et al., 2015; Trotter et al., 2016). Differences between crowns and roots (Fig. SM-3), including higher U concentrations in roots, further support the idea that porous, organic-rich tissues are more prone to incorporating terrigenous material. The different R -values of the crowns and roots (R^2 is higher for roots; Fig. SM-3) may be due to the presence of terrigenous residues inside the more porous root structure (Al, Fe and Sr values are on average higher in the roots). The occurrence of terrigenous material inside the roots could also be confirmed by their U content, which varies widely across the samples and does not provide relevant outliers. In fact, U abundances range between 0.02 and 1.65 ppm (average value of 0.60 ppm) for crowns and between 0.15 and 9.47 ppm (average 2.34 ppm) for roots, regardless of their age and depositional/diagenetic setting. All these features have practical implications: the crown enameloid may preserve near-original crystallinity comparable to extant analogues (Fig. 7), roots are less reliable for paleoenvironmental reconstructions.

The initial assessment using the CI showed high variability and overlap between extant and fossil crowns. However, utilizing

crystallographic size parameters substantially improved the crystallinity distinction, indicating that fossil crowns have slightly higher crystallinity. This finding supports the hypothesis that the presence of a minimal amount of organic matter in extant shark crowns is sufficient to cause a corresponding slight reduction in crystallinity.

Crystallographic size parameters further highlight functional contrasts. Fossil crowns exhibit larger crystallite widths and lengths compared to roots, indicating enhanced crystallinity due to carbon incorporation (Fig. 8). Results for the fossil samples, as well as for the crowns and scales of extant sharks, highlight a preference for bioapatite to crystallize along the direction defined by the c axis. This behavior could be due to the texture and shape of these elements, which also characterizes the roots of the fossil elements, despite the completely random orientation of their crystallites, as highlighted by their Debye rings in the bidimensional images of X-ray diffraction signals.

The orientation-related scatter of crown crystallites may be linked to biomechanical demands, where variability in crystallite size enhances durability and resistance to fracture during feeding. In contrast, shark scales displayed crystallites with more uniform dimensions (width \approx length; Fig. 8), supporting the interpretation that scales follow a homogeneous mineralization pattern optimized for hydrodynamic efficiency and body protection.

Peculiar results are provided by the fossil roots of the extinct shark *P. distans*: according to the Student t -test (p -value always <0.01), these samples exhibit higher CI (Fig. 7), width, length, $N_{\text{UnitCell}(a)}$, and $N_{\text{UnitCell}(c)}$ (Fig. 8) values compared to other fossil roots. These differences are relevant considering that CI (on the one hand) and the size parameters width, length, $N_{\text{UnitCell}(a)}$, and $N_{\text{UnitCell}(c)}$ (on the other hand) were calculated following different procedures and, as such, are not correlated with each other. Both sets of values highlight a greater crystallinity of the root of *P. distans* which may reflect either a different physiological characteristics or different diagenetic conditions for the teeth of *P. distans* compared to all other samples. Conversely, the geological age (Middle Miocene) of these teeth has no significant bearing on the results, as this study analyzed both older and younger fossil materials. Despite this overprint, the Ce/Ce^* vs Pr/Pr^* diagram (Fig. 11) shows clustering of samples by geological age, indicating that depositional redox conditions still left an imprint on the REE patterns. For example, slight positive Ce and La anomalies in Miocene samples, and weak negative La anomalies in Eocene samples, point to redox variability in their burial environments. Thus, although REE systematics cannot be taken as pristine seawater archives, they remain useful indicators of the diagenetic environment as demonstrated in different marine and terrestrial settings (e.g., Suarez et al., 2010; Trueman et al., 2011; Ullmann et al., 2020).

Extant sharks also displayed intriguing REE signals. In *G. melastomus*, weak positive Ce and La anomalies (Fig. 13) may reflect local seawater chemistry, biological uptake preferences, or other biogeochemical controls. However, the very low REE concentrations in *S. canicula* (often near detection limits) produced more scattered correlations (Fig. 12), suggesting interspecific differences in uptake or physiological regulation. Unfortunately, the lack of literature data precludes a conclusion as to whether this anomaly reflects the complex interactions between the chemistry of the surrounding water and subtle biological control over trace element incorporation into shark bioapatite. The observation of similar correlative patterns among other elements (e.g., Fe and Mn; Fig. SM-4) further highlights this uncertainty.

7. Conclusions

The present study enabled a comparative analysis of the crystallographic and chemical properties of fossilized bioapatite in catsharks from different geological ages and locations relative to those observed in their modern counterparts. Diagenetic processes led to the loss of the organic matter that was originally present in living bioapatites, which was accompanied by a proportional increase of the carbon content of the

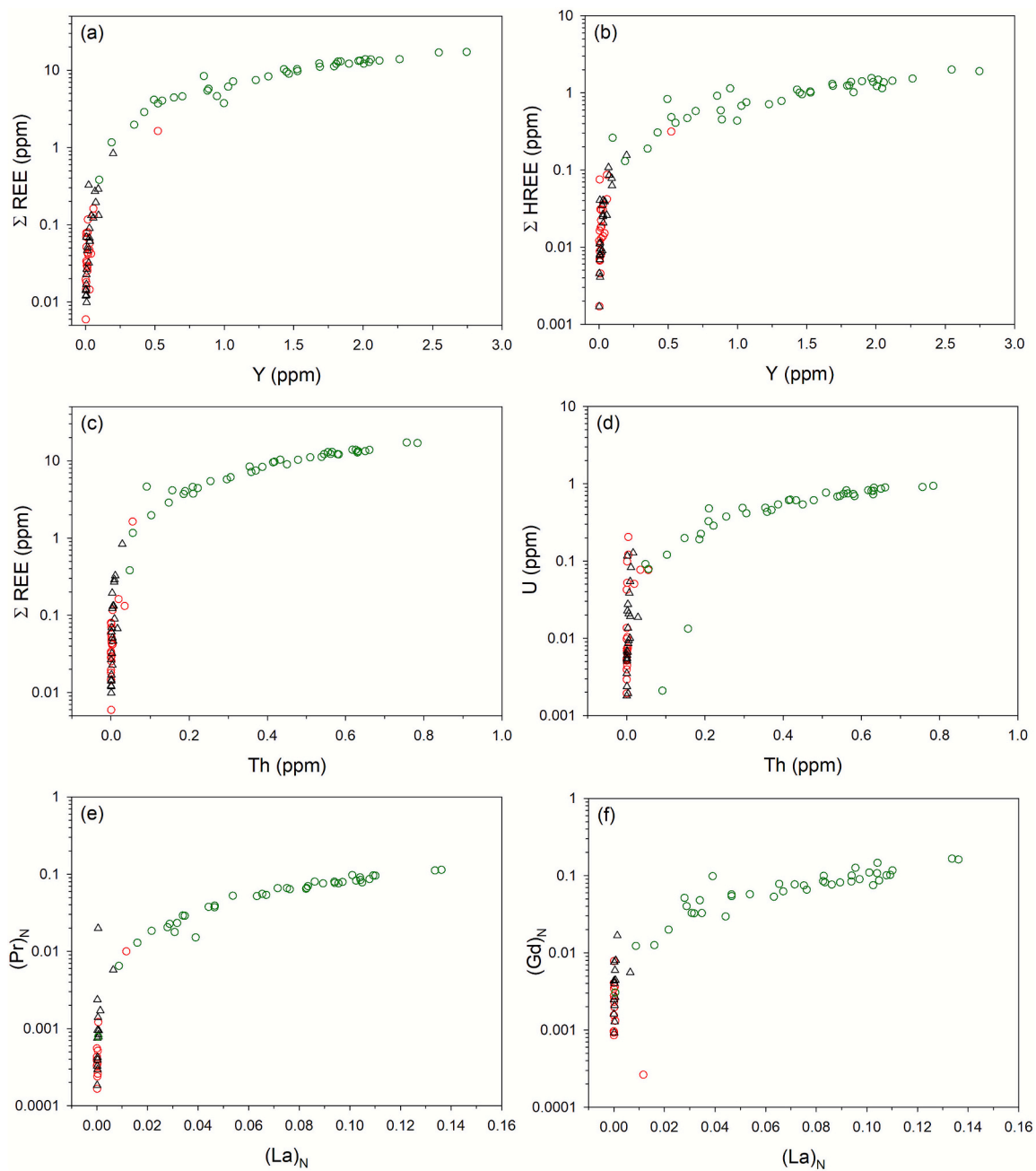


Fig. 12. Crossplots of ΣREE and ΣHREE vs Y (a and b), ΣREE vs Th (c), U vs Th (d), (Pr)_N vs (La)_N (e) and (Gd)_N vs (La)_N (f) in *Scyliorhinus canicula* crown (red circles), *Galeus melastomus* crown (green circles) and *Scyliorhinus canicula* scales (triangles). (For interpretation of the references to colour in this figure legend, the reader is referred to the web version of this article.)

bioapatite framework. Notably, the greater the initial organic matter in specific regions of the teeth living sharks, the higher the carbon concentration observed in the corresponding fossilized structures. The presence of carbon in the fossil samples is directly associated with a reduction of the *a* lattice parameter and unit cell volume, as well as with an increase of the *c* parameter and overall crystallinity. Tooth crowns exhibited higher values of the *a* lattice parameter, unit cell volume and crystallinity compared to tooth roots, which can be attributed to their lower organic matter content in living sharks and reduced carbon incorporation during diagenesis. However, the modest presence of organic matter in the crowns of living sharks may be sufficient to explain their slightly lower crystallinity compared to their fossilized counterparts. Fossilized tooth roots exhibit the most pronounced deviations from their modern counterparts, reflecting the significant impact of the

diagenetic processes. These alterations primarily affected the organic components of the teeth, resulting in enhanced crystallinity throughout the structure.

The influence of diagenetic processes on these samples appears to be independent of their geological age. Variations observed in specific fossil specimens may reflect differences in the corresponding depositional and/or diagenetic environments; however, a potential contribution of physiological traits inherent to the living organisms cannot be excluded straightforward.

Crystallographic analyses revealed that the scales of the living sharks possess crystallites with relatively uniform dimensions along both the *a* and *c* crystallographic axes, suggesting a structurally homogeneous mineral organization. In contrast, tooth samples exhibit a more variable crystallite size distribution, likely reflecting different functional

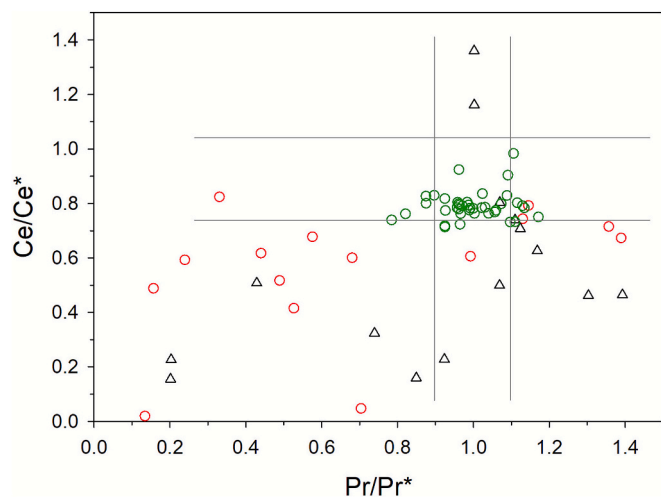


Fig. 13. Location of the Recent samples in the McLennan (2001) normalized plots of (Ce/Ce^*) vs (Pr/Pr^*) . Adapted from Kowal-Linka et al. (2014). Symbols correspond to those shown in Fig. 12.

adaptations. This variability may be linked to the specific mechanical demands of each tooth position during predation, where optimized crystallite orientation and size contribute to enhanced durability, resistance to fracture, and overall biomechanical efficiency. Such differentiation underscores the role of tissue-specific biomineralization strategies in elasmobranch skeletal elements, which have been shaped by evolutionary pressures and ecological requirements over the last 250 million years or so.

Taken together, our results demonstrate that bioapatite records both primary biological signals (e.g., tissue-specific crystallite organization, functional adaptations of scales vs teeth) and secondary diagenetic overprints (e.g., REE enrichment, lattice contraction). To the geochemist, this study provides a cautionary tale: interpretations of REE systematics in fossil bioapatite must account for diagenetic signatures, though age-related patterns still encode valuable environmental information. To the paleontologist, it warns that shark teeth and scales are not just phylogenetic or taxonomic markers, but also archives of tissue-specific mineralization strategies shaped by evolutionary pressures.

CRediT authorship contribution statement

Luca Medici: Writing – review & editing, Writing – original draft, Visualization, Validation, Supervision, Resources, Project administration, Methodology, Investigation, Formal analysis, Data curation, Conceptualization. **Annalisa Ferretti:** Writing – review & editing, Writing – original draft, Visualization, Validation, Supervision, Resources, Investigation, Funding acquisition, Formal analysis, Data curation, Conceptualization. **Alberto Collareta:** Writing – review & editing, Writing – original draft, Visualization, Validation, Supervision, Resources, Investigation, Funding acquisition, Formal analysis, Data curation, Conceptualization. **Giulia Bosio:** Writing – original draft, Visualization, Resources, Investigation, Data curation. **Giovanni Bianucci:** Writing – original draft, Visualization, Resources, Investigation, Data curation. **Giorgio Carnevale:** Writing – original draft, Visualization, Validation, Resources, Investigation, Data curation, Conceptualization. **Simone Casati:** Writing – original draft, Visualization, Resources, Investigation, Data curation. **Simona Clò:** Writing – original draft, Visualization, Resources, Methodology, Investigation, Data curation. **Luca Lanteri:** Writing – original draft, Visualization, Resources, Methodology, Investigation, Data curation. **Federico Lugli:** Writing – original draft, Visualization, Resources, Investigation, Data curation. **Giuseppe Marramà:** Writing – original draft, Visualization, Resources, Investigation, Funding acquisition, Data curation. **Frederik H. Mollen:**

Writing – original draft, Visualization, Resources, Investigation, Data curation. **Martina Savioli:** Writing – original draft, Visualization, Resources, Methodology, Investigation, Formal analysis, Data curation. **Daniele Malferrari:** Writing – review & editing, Writing – original draft, Visualization, Validation, Supervision, Resources, Methodology, Investigation, Formal analysis, Data curation, Conceptualization.

Declaration of competing interest

The authors declare the following financial interests/personal relationships which may be considered as potential competing interests:

Alberto Collareta reports financial support was provided by Italian Ministry of University and Research (MUR). If there are other authors, they declare that they have no known competing financial interests or personal relationships that could have appeared to influence the work reported in this paper.

Acknowledgements

We are grateful to the Scientific Instruments Facility, CIGS (University of Modena and Reggio Emilia, Italy), and especially to Daniela Manzini and Lisa Lancellotti for LA-ICPMS expertise. We acknowledge financial support under the National Recovery and Resilience Plan (PNRR), Mission 4, Component 2, Investment 1.1, Call for tender No. 104 published on 02/02/2022 by the Italian Ministry of University and Research (MUR), funded by the European Union – NextGeneration EU – Project Title: BIOVERTICES (BIOdiversity of VERtebrates In the CEEnozoic Sea) - CUP I53D23002070 006 - Grant Assignment Decree No. 965 adopted on 30/06/2023 by the Italian Ministry of University and Research (MUR).

Appendix A. Supplementary data

Supplementary data to this article can be found online at <https://doi.org/10.1016/j.chemgeo.2025.123200>.

Data availability

All data are included in the paper

References

- Abella, A., Serena, F., 2002. Comparison of Elasmobranch Catches of Trawl Surveys and Commercial Landings of the Port of Viareggio (North Tyrrhenian - South Ligurian Sea, Italy) in the Last Decade. Technical Document. NAFO Council Meeting, Santiago de Compostela (Spain). September 2002.
- Abella, A., Mancusi, C., Mannini, A., Serena, F., 2017a. *Galeus melastomus*. In: Sartor, P., Mannini, A., Carlucci, R., Massaro, E., Queirolo, S., Sabatini, A., Scarcella, G., Simoni, R. (Eds.), Sintesi delle conoscenze di biologia, ecologia e pesca delle specie ittiche dei mari italiani. Biol. Mar. Mediterr. 24 (Suppl. 1), 136–143.
- Abella, A., Mancusi, C., Serena, F., 2017b. *Scyliorhinus canicula*. In: Sartor, P., Mannini, A., Carlucci, R., Massaro, E., Queirolo, S., Sabatini, A., Scarcella, G., Simoni, R. (Eds.), Sintesi delle conoscenze di biologia, ecologia e pesca delle specie ittiche dei mari italiani. Biol. Mar. Mediterr. 24 (Suppl. 1), 157–164.
- Antunes, M.T., Jonet, S., 1970. Requis de l'Helvétien supérieur et du Tortonien de Lisbonne. Rev. Fac. Cienc. Univ. Lisboa 16, 119–280.
- Armstrong, H.A., Pearson, D.G., Griselin, M., 2001. Thermal effects on rare earth element and strontium isotope chemistry in single conodont elements. Geochim. Cosmochim. Acta 65, 435–441.
- Baino, R., Serena, F., Ragonese, S., Rey, J., Rinelli, P., 2001. Catch composition and abundance of Elasmobranchs based on the MEDITS program. Rapp. Comm. Intern. pour l'explor. Scien. Méditerr. (CIESM) 36, 234.
- Bánki, O., Roskov, Y., Döring, M., Ower, G., Hernández Robles, D.R., Plata Corredor, C. A., Stjernegaard Jeppesen, T., Örn, A., Pape, T., Hobern, D., Garnett, S., Little, H., DeWalt, R.E., Ma, K., Miller, J., Orrell, T., Aalbu, R., Abbott, J., Aedo, C., et al., 2024. Catalogue of Life (Version 2024-12-19). Catalogue of Life, Amsterdam, Netherlands.
- Benoit, J., Adnet, S., Welcomme, J.L., Fabre, P.H., 2011. New skull of *Schizodelphis sulcatus* Gervais, 1861 (Mammalia, Odontoceti, Eurhinodelphinidae) from the Lower Miocene of Pignan (Hérault, France) and its implications for systematics of Eurhinodelphinidae. Geobios 44, 323–334.
- Benton, M.J., Harper, D.A.T., 2009. Introduction to Paleobiology and the Fossil Record. John Wiley & Sons Ltd.

- Berkovitz, B., Shells, P., 2017. The Teeth of Non-mammalian Vertebrates. Academic Press.
- Bianucci, G., Pesci, F., Collareta, A., Tinelli, C., 2019. A new Monodontidae (Cetacea, Delphinoidea) from the lower Pliocene of Italy supports a warm-water origin for narwhals and white whales. *J. Vertebr. Paleontol.* 39, e1645148.
- Bosio, G., Giocada, A., Gariboldi, K., Bonaccorsi, E., Collareta, A., Pasero, M., Di Celma, C., Malinverno, E., Urbina, M., Bianucci, G., 2021. Mineralogical and geochemical characterization of fossil bones from a Miocene marine Konservat-Lagerstätte. *J. S. Am. Earth Sci.* 105, 102924.
- Bosio, G., Bianucci, G., Collareta, A., Landini, W., Urbina, M., Di Celma, C., 2022. Ultrastructure, composition, and $^{87}\text{Sr}/^{86}\text{Sr}$ dating of shark teeth from lower Miocene sediments of southern Peru. *J. S. Am. Earth Sci.* 118, 103909.
- Brée, B., Condamine, F.L., Guinot, G., 2022. Combining palaeontological and neontological data shows a delayed diversification burst of carcharhiniform sharks likely mediated by environmental change. *Sci. Rep.* 12, 21906.
- Cacciotti, I., 2016. Cationic and Anionic Substitutions in Hydroxyapatite. In: *Handbook of Bioceramics and Biocomposites*. Springer International Publishing Switzerland, I. V. Antoniac, pp. 145–211.
- Cappetta, H., 1970. Les séliaciens du Miocène de la région de Montpellier. *Palaeovertebrata. Mém. Extr.* 1970, 1–139.
- Cappetta, H., 1976. Séliaciens nouveaux du London Clay de l'Essex (Yprésien du bassin de Londres). *Geobios* 9, 551–575.
- Cappetta, H., 2012. Chondrichthyes. Mesozoic and Cenozoic Elasmobranchii Teeth. Pfeil-Verlag, Munich.
- Chen, J., Algeo, T.J., Zhao, L., Chen, Z.-Q., Cao, L., Zhang, L., Li, Y., 2015. Diagenetic uptake of rare earth elements by bioapatite, with an example from Lower Triassic conodonts of South China. *Earth-Sci. Rev.* 149, 181–202.
- Cione, A.L., 1986. A new *Megascyliorhinus* (Chondrichthyes, Galeomorphii) from the middle Tertiary of Patagonia. *J. Vertebr. Paleontol.* 6, 105–112.
- Collareta, A., Merella, M., Casati, S., Di Cencio, A., 2021a. First fossils of the extant blacktip shark *Carcharhinus limbatus* from Europe and the Mediterranean Basin. *Neues Jahrb. Geol. Palaontol. Abh.* 301, 109–118.
- Collareta, A., Mollen, F.H., Merella, M., Casati, S., Di Cencio, A., 2021b. Remarkable multicuspoid teeth in a new elusive skate (Chondrichthyes, Rajiformes) from the Mediterranean Pliocene. *PalZ* 95, 117–128.
- Compagno, L.J.V., 1984. Squaliformes-Dogfish sharks. In: Fischer, W., Nauen, C. (Eds.), *FAO Species Catalogue, volume 4. Sharks of the World: An Annotated and Illustrated Catalogue of Shark Species Known to Date. Part I. Hexanchiformes to Lamniformes, 125. FAO Fisheries Synopsis, Rome, pp. 1–249.*
- Compagno, L.J.V., 1988. *Sharks of the Order Carcharhiniformes*. Princeton University Press, Princeton, NJ.
- Cuny, G., Guinot, G., Enault, S., 2017. *Evolution of Dental Tissues and Paleobiology in Selachians*. Elsevier.
- Dal Sasso, G., Asscher, Y., Angelini, I., Nodari, L., Artioli, G., 2018. A universal curve of apatite crystallinity for the assessment of bone integrity and preservation. *Sci. Rep.* 8, 12025.
- Dominici, S., Forli, M., 2021. Lower Pliocene molluscs from southern Tuscany (Italy). *Boll. Soc. Paleontol. Ital.* 60, 69–98.
- Dumont, M., Kostka, A., Sander, P.M., Borbely, A., Kaysser-Pyzalla, A., 2011. Size and size distribution of apatite crystals in sauroid fossil bones. *Palaeogeogr. Palaeoclimatol. Palaeoecol.* 310, 108–116.
- Enax, J., Prymak, O., Raabe, D., Epple, M., 2012. Structure, composition, and mechanical properties of shark teeth. *J. Struct. Biol.* 178 (3), 290–299.
- Ferretti, A., Malferrari, D., Medici, L., Savioli, M., 2017. Diagenesis does not invent anything new: Precise replication of conodont structures by secondary apatite. *Sci. Rep.* 7, 1624.
- Ferretti, A., Medici, L., Savioli, M., Mascia, M.T., Malferrari, D., 2021. Dead, fossil or alive: Bioapatite diagenesis and fossilization. *Palaeogeogr. Palaeoclimatol. Palaeoecol.* 579, 110608.
- Ferretti, A., Corradini, C., Fakir, S., Malferrari, D., Medici, L., 2023. To be or not to be a conodont. The controversial story of *Pseudoneotodus* and *Eurytholia*. *Mar. Micropaleontol.* 182, 102258.
- Finucci, B., Derrick, D., Neat, F.C., Pacoureaux, N., Serena, F., VanderWright, W.J., 2021a. *Galeus melastomus*. The IUCN Red list of Threatened Species 2021 e. T161398A124477972.
- Finucci, B., Derrick, D., Neat, F.C., Pacoureaux, N., Serena, F., VanderWright, W.J., 2021b. *Scyliorhinus canicula*. The IUCN Red list of Threatened Species 2021 e. T161307554A124478351.
- Fischer, J., Schneider, J.W., Voigt, S., Joachimski, M.M., Tichomirowa, M., Tütken, T., Götze, J., Berner, U., 2013. Oxygen and strontium isotopes from fossil shark teeth: environmental and ecological implications for late Palaeozoic European basins. *Chem. Geol.* 342, 44–62.
- Follesa, M.C., Carbonara, P. (Eds.), 2019. *Atlas of the Maturity Stages of Mediterranean Fishery Resources. Studies and Reviews, vol. 99. FAO, Rome.*
- Fraser, G.J., Hulsey, C.D., 2020. Biology at the cusp: teeth as a model phenotype for integrating developmental genomics, biomechanics, and ecology. *Integr. Comp. Biol.* 60, 559–562.
- Froese, R., Pauly, D. (Eds.), 2024. *FishBase. World Wide Web electronic publication. www.fishbase.org.*
- Girard, C., Albarède, F., 1996. Trace elements in conodont phosphates from the Frasnian/Famennian boundary. *Palaeogeogr. Palaeoclimatol. Palaeoecol.* 126, 195–209.
- Glickman, L.S., 1964. Class Chondrichthyes, subclass Elasmobranchii. In: *Bruce, D.V. (Ed.), Fundamental of Paleontology. Nauka SSSR, Moscow-Leningrad, pp. 196–237.*
- Grandjean, P., Cappetta, H., Michard, A., Albarède, F., 1987. The assessment of REE patterns and $^{143}\text{Nd}/^{144}\text{Nd}$ ratios in fish remains. *Earth Planet. Sci. Lett.* 84, 181–196.
- Grandjean-Lécuyer, P., Feist, R., Albarède, F., 1993. Rare earth elements in old biogenic apatites. *Geochim. Cosmochim. Acta* 57, 2507–2514.
- Herwartz, D., Tütken, T., Münker, C., Jochum, K.P., Stoll, B., Sander, P.M., 2011. Timescales and mechanisms of REE and Hf uptake in fossil bones. *Geochim. Cosmochim. Acta* 75, 82–105.
- Herwartz, D., Tütken, T., Jochum, K.P., Sander, P.M., 2013. Rare earth element systematics of fossil bone revealed by LA-ICPMS analysis. *Geochim. Cosmochim. Acta* 103, 161–183.
- Holland, T.J.B., Redfern, S.A.T., 1997. Unit cell refinement from powder diffraction data: the use of regression diagnostics. *Mineral. Mag.* 61, 65–77.
- Holser, W.T., 1997. Evaluation of application of rare-earth elements to paleoceanography. *Palaeogeogr. Palaeoclimatol. Palaeoecol.* 132, 309–323.
- Iglésias, S.P., Lecointre, G., Sellos, D.Y., 2005. Extensive paraphyly within sharks of the order Carcharhiniformes inferred from nuclear and mitochondrial genes. *Mol. Phylogenet. Evol.* 34, 569–583.
- IUCN, 2025. *The IUCN Red list of Threatened Species. Version 2025-2. https://www.iucnredlist.org.*
- Jambura, P.L., Pfaff, C., Underwood, C.J., Ward, D.J., Kriwet, J., 2018. Tooth mineralization and histology patterns in extinct and extant snaggletooth sharks, Hemipristis (Carcharhiniformes, Hemigaleidae) - evolutionary significance or ecological adaptation? *PLoS One* 13 (8), e0200951.
- Jambura, P.L., Türtscher, J., Kindlimann, R., Metscher, B., Pfaff, C., Stumpf, S., Weber, G. W., Kriwet, J., 2020. Evolutionary trajectories of tooth histology patterns in modern sharks (Chondrichthyes, Elasmobranchii). *J. Anat.* 236 (5), 753–771.
- Kim, J.-H., Torres, M.E., Haley, B.A., Kastner, M., Pohlman, J.W., Riedel, M., Lee, Y.-J., 2012. The effect of diagenesis and fluid migration on rare earth element distribution in pore fluids of the northern Cascadia accretionary margin. *Chem. Geol.* 291, 152–165.
- Kocsis, L., Trueman, C.N., Palmer, M.R., 2010. Protracted diagenetic alteration of REE contents in fossil bioapatites: Direct evidence from Lu-Hf isotope systematics. *Geochim. Cosmochim. Acta* 74, 6077–6092.
- Kowal-Linka, M., Jochum, K.P., Surmik, D., 2014. LA-ICP-MS analysis of rare earth elements in marine reptile bones from the Middle Triassic bonebed (Upper Silesia, S Poland): impact of long-lasting diagenesis, and factors controlling the uptake. *Chem. Geol.* 363, 213–228.
- Lawley, R., 1876. *Nuovi studi sopra i pesci ed altri vertebrati fossili delle colline Toscane. Tipografia dell'Arte della Stampa, Firenze.*
- Lécuyer, C., Reynard, B., Grandjean, P., 2004. Rare earth element evolution of Phanerozoic seawater recorded in biogenic apatites. *Chem. Geol.* 204, 63–102.
- Liao, J., Sun, X., Li, D., Sa, R., Lu, Y., Lin, Z., Xu, L., Zhan, R., Pan, Y., Xu, H., 2019. New insights into nanostructure and geochemistry of bioapatite in REE-rich deep-sea sediments: LA-ICP-MS, TEM, and Z-contrast imaging studies. *Chem. Geol.* 512, 58–68.
- Linnaeus, 1758. *Systema Naturae per regna tria naturae, regnum animale, secundum classes, ordines, genera, species, cum characteribus differentis synonymis, locis. Tomus I. Editio decima, reformata. Holmiae, Impensis Direct, Laurentii Salvii.*
- Lowenstam, H.A., Weiner, S., 1989. *On biomineralization*. Oxford University Press.
- Malferrari, D., Ferretti, A., Mascia, M.T., Savioli, M., Medici, L., 2019. How much can we trust major element quantification in bioapatite investigation? *ACS Omega* 4, 17814–17822.
- Malferrari, D., Ferretti, A., Medici, L., 2024. The origin and significance of euhedral apatite crystals on conodonts. *Mar. Micropaleontol.* 186, 102308.
- Manganelli, G., Spadini, V., 2019. *Megascyliorhinus miocaenicus* (Chondrichthyes, Galeomorphii) from the Zanclean (early Pliocene) of San Quirico d'Orcia, central Italy. *Boll. Soc. Paleontol. Ital.* 58, 165–170.
- Martini, L., Sandrelli, F., 2015. Facies analysis of a Pliocene river-dominated deltaic succession (Siena Basin, Italy): Implications for the formation and infilling of terminal distributary channels. *Sedimentology* 62, 234–265.
- Martini, I.P., Sagri, M., 1993. Tectono-sedimentary characteristics of Late Miocene-Quaternary extensional basins of the Northern Apennines, Italy. *Earth-Sci. Rev.* 34, 197–233.
- McLennan, S.M., 2001. Relationships between the trace element composition of sedimentary rocks and upper continental crust. *Geochem. Geophys. Geosyst.* 2, 2000GC000109.
- Medici, L., Malferrari, D., Savioli, M., Ferretti, A., 2020. Mineralogy and crystallization patterns in conodont bioapatite from first occurrence (Cambrian) to extinction (end-Triassic). *Palaeogeogr. Palaeoclimatol. Palaeoecol.* 549, 109098.
- Medici, L., Savioli, M., Ferretti, A., Malferrari, D., 2021. Zooming in REE and other trace elements on conodonts: Does taxonomy guide diagenesis? *J. Earth Sci.* 32, 501–511.
- Merella, M., Collareta, A., Casati, S., Di Cencio, A., Bianucci, G., 2023. Pliocene Geotourism: Innovative Projects for Valorizing the Paleontological Heritage of Three Different-Stage Quarries of Tuscany (Central Italy). *Geoheritage* 15, 82.
- Mollen, F.H., 2019. Making Louis Agassiz's wish come true: combining forces and a new protocol for collecting comparative skeletal material of sharks, skates and rays, as a comment and an addition to 'The need of providing tooth morphology in descriptions of extant elasmobranch species' by Guinot et al. (2018). *Zootaxa* 4571, 295–300.
- Moyer, J.K., Riccio, M.L., Bemis, W.E., 2015. Development and microstructure of tooth histotypes in the blue shark, *Prionace glauca* (Carcharhiniformes: carcharhinidae) and the great white shark, *Carcharodon carcharias* (Lamniformes: Lamnidae). *J. Morphol.* 276 (7), 797–817.
- Mytilineou, Ch., Politou, C.-Y., Papaconstantinou, C., Kavadas, S., D'Onghia, G., Sion, L., 2005. Deep-water fish fauna in the Eastern Ionian Sea. *Belg. J. Zool.* 135, 229–233.
- Nardelli, M.P., Malferrari, D., Ferretti, A., Bartolini, A., Sabbatini, A., Negri, A., 2016. Zinc incorporation in the miliolid foraminifer *Pseudotriloculina rotunda* under laboratory conditions. *Mar. Micropaleontol.* 126, 42–49.

- Nothdurft, L.D., Webb, G.E., Kamber, B.S., 2004. Rare earth element geochemistry of Late Devonian reefal carbonates, Canning Basin, Western Australia: confirmation of a seawater REE proxy in ancient limestones. *Geochim. Cosmochim. Acta* 68, 263–283.
- Ørving, T., 1951. Histologic studies of placoderms and fossil elasmobranchs. *Ark. Zool.* 2, 321–454.
- Pattan, J.N., Pearce, N.J.G., Mislankar, P.G., 2005. Constraints in using cerium-anomaly of bulk sediments as an indicator of paleo bottom water redox environment: a case study from the Central Indian Ocean Basin. *Chem. Geol.* 221, 260–278.
- Peppe, D.J., Reiners, P.W., 2007. Conodont (U-Th)/He thermochronology: initial results, potential, and problems. *Earth Planet. Sci. Lett.* 258, 569–580.
- Person, A., Bocherens, H., Saliège, J.F., Paris, F., Zeitoun, V., Gérard, M., 1995. Early Diagenetic Evolution of Bone Phosphate: An X-Ray Diffractometry Analysis. *J. Archaeol. Sci.* 22, 211–221.
- Picard, S., Lécuyer, C., Barrat, J.A., Garcia, J.-P., Dromart, G., Sheppard, S.M.F., 2002. Rare earth element contents of Jurassic fish and reptile teeth and their potential relation to seawater composition (Anglo-Paris basin, France and England). *Chem. Geol.* 186, 1–16.
- Pietsch, C., Bottjer, D.J., 2010. Comparison of changes in ocean chemistry in the early Triassic with trends in diversity and ecology. *J. Earth Sci.* 21, 147–150.
- Pinto, C., Mannini, A., Relini, G., 2010. Remarks on *Galeus melastomus* in the northern Ligurian sea. *Biol. Mar. Mediterr.* 17, 224–227.
- Probst, J., 1879. Beiträge zur Kenntniss der fossilen Fische aus der Molasse von Baltringen. *Hayfische. Jahresh. Ver. vaterl. Naturkd. Wb.* 35, 127–191.
- Rafinesque, C.S., 1810. Caratteri di alcuni nuovi generi e nuove specie di animali e piante della Sicilia, con varie osservazioni sopra i medesimi. Per le stampe di Sanfilippo, Palermo, Italy.
- Reinecke, T., Mollen, F.H., Gijssen, B., D'Haese, B., Hoedemakers, K., 2024. Batomorphs (Elasmobranchii: Rhinopristiformes, Rajiformes, Torpediniformes, Myliobatiformes) of the middle to late Ypresian, early Eocene, in the Anglo-Belgian Basin (south-western North Sea Basin)—a review and description of new taxa. *Palaeontol.* 35, 3–171.
- Relini, G., 2007. La pesca batiale in Liguria. *Biol. Mar. Mediterr.* 14, 190–244.
- Reynard, B., Lécuyer, C., Grandjean, P., 1999. Crystal-chemical controls on rare earth element concentrations in fossil biogenic apatites and implications for paleoenvironmental reconstructions. *Chem. Geol.* 155, 233–241.
- Senter, P.J., 2022. Cells and soft tissues in fossil bone: a review of preservation mechanisms, with corrections of misconceptions. *Palaeontol. Electron.* 25, a34.
- Serena, F., Abella, A.J., Bargnesi, F., Barone, M., Colloca, F., Ferretti, F., Fiorentino, F., Jenrette, J., Moro, S., 2020. Species diversity, taxonomy and distribution of Chondrichthyes in the Mediterranean and Black Sea. *Eur. Zool. J.* 87, 497–536.
- Shen, J., Algeo, T.J., Zhou, L., Feng, Q., Yu, J., Ellwood, B., 2012. Volcanic perturbations of the marine environment in South China preceding the latest Permian mass extinction and their biotic effects. *Geobiology* 10, 82–103.
- Shirley, B., Leonhard, I., Murdock, D.J.E., Repetski, J., Świś, P., Bestmann, M., Trimby, P., Ohl, M., Plümpner, O., King, H.E., Jarochovska, E., 2024. Increasing control over biomineralization in conodont evolution. *Nat. Commun.* 15, 5273.
- Smith, T., Smith, R., 2013. A land micro-mammal fauna from the Early Eocene marine Egem deposits (NP12, Belgium) and the first occurrence of the peradectid marsupial *Arminodelphys* outside North America. *Geol. Belg.* 16, 302–310.
- Soares, K.D., Mathubara, K., 2022. Combined phylogeny and new classification of catsharks (Chondrichthyes: Elasmobranchii: Carcharhiniformes). *Zool. J. Linnean Soc.* 195, 761–814.
- Song, H., Wignall, P.B., Song, H., Dai, X., Chu, D., 2019. Seawater Temperature and Dissolved Oxygen over the Past 500 Million Years. *J. Earth Sci.* 30, 236–243.
- Sorbi, S., Domning, D.P., Vaiani, S.C., Bianucci, G., 2012. *Metaxytherium subapenninum* (Bruno, 1839) (Mammalia, Dugongidae), the latest sirenian of the Mediterranean Basin. *J. Vertebr. Paleontol.* 32, 686–707.
- Steurbaut, E., 1988. Ypresian calcareous nannoplankton biostratigraphy and palaeogeography of the Belgian Basin. The Ypresian stratotype. *Bull. Belg. Ver. Geol.* 97, 251–285.
- Steurbaut, E., 1998. High-resolution holostratigraphy of Middle Paleocene to Early Eocene strata in Belgium and adjacent areas. *Palaeontogr. Abt. A* 247, 91–156.
- Steurbaut, E., 2006. Ypresian. *Geol. Belg.* 9, 73–93.
- Suarez, C.A., Macpherson, G.L., Gonzalez, L.A., Grandstaff, D.E., 2010. Heterogeneous rare earth element (REE) patterns and concentrations in a fossil bone: implications for the use of REE in vertebrate taphonomy and fossilization history. *Geochim. Cosmochim. Acta* 74, 2970–2988.
- Suarez, M., Encinas, A., Ward, D., 2004. An Early Miocene elasmobranch fauna from the Navidad Formation, Central Chile, South America. *Cainozoic Res.* 4, 3–18.
- Thies, D., 2005. A catshark (Neoselachii, Carcharhiniformes, Scyliorhinidae) from the Late Jurassic of Germany. *PalZ* 79, 339–348.
- Toyoda, K., Tokonami, M., 1990. Diffusion of rare-earth elements in fish teeth from deep-sea sediments. *Nature* 345, 607–609.
- Trotter, J.A., Eggins, S.M., 2006. Chemical systematics of conodont apatite determined by laser ablation ICPMS. *Chem. Geol.* 233, 196–216.
- Trotter, J.A., Barnes, C.R., McCracken, A.D., 2016. Rare earth elements in conodont apatite: Seawater or pore-water signatures? *Palaeogeogr. Palaeoclimatol. Palaeoecol.* 462, 92–100.
- Trueman, C.N., Kocsis, L., Palmer, M.R., Dewdney, C., 2011. Fractionation of rare earth elements within bone mineral: a natural cation exchange system. *Palaeogeogr. Palaeoclimatol. Palaeoecol.* 310, 124–132.
- Ullmann, P.V., Grandstaff, D.E., Ash, R.D., Lacovara, K.J., 2020. Geochemical taphonomy of the Standing Rock Hadrosaur Site: Exploring links between rare earth elements and cellular and soft tissue preservation. *Geochim. Cosmochim. Acta* 269, 223–237.
- Underwood, C.J., 2006. Diversification of the Neoselachii (Chondrichthyes) during the Jurassic and Cretaceous. *Paleobiology* 32, 215–235.
- Vacchi, M., Serena, F., 2010. Chondrichthyes. In: Relini, G. (Ed.), Checklist della flora e della fauna dei mari italiani, 17 (Suppl. 1). Parte II. *Biol. Mar. Mediterr.*, pp. 642–648.
- Vennemann, T.W., Hegner, E., Cliff, G., Benz, G.W., 2001. Isotopic composition of recent shark teeth as a proxy for environmental conditions. *Geochim. Cosmochim. Acta* 65 (10), 1583–1599.
- Villalobos-Segura, E., Stumpf, S., Türtscher, J., Jambura, P.L., Begat, A., López-Romero, F.A., Fischer, J., Kriwet, J., 2023. A synoptic review of the cartilaginous fishes (Chondrichthyes: Holocephali, Elasmobranchii) from the Upper Jurassic Konservat-Lagerstätten of southern Germany: taxonomy, diversity, and faunal relationships. *Diversity* 15, 386.
- Wagner, J.A., 1857. Charakteristik neuer Arten von Knorpelfischen aus den lithographischen Schiefer der Umgegend von Solnhofen. *Gel. Anz. Königl. Bayer. Akad. Wiss.* 44, 288–293.
- Webb, G.E., Kamber, B.S., 2000. Rare earth elements in Holocene reefal microbialites: a new shallow seawater proxy. *Geochim. Cosmochim. Acta* 64, 1557–1565.
- Webb, G.E., Nothdurft, L.D., Kamber, B.S., Klopogge, J.T., Zhao, J.X., 2009. Rare earth element geochemistry of scleractinian coral skeleton during meteoric diagenesis: a sequence through neomorphism of aragonite to calcite. *Sedimentology* 56, 1433–1463.
- Weigmann, S., 2016. Annotated checklist of the living sharks, batoids and chimaeras (Chondrichthyes) of the world, with a focus on biogeographical diversity. *J. Fish Biol.* 88, 837–81037.
- Weiner, S., Dove, P.M., 2023. An overview of biomineralization processes and the problem of the vital effect. *Rev. Mineral. Geochem.* 54, 1–29.
- White, W.T., Stewart, A.L., O'Neill, H.L., Naylor, G.J.P., 2024. Dichichthyidae, a New Family of Deepwater Sharks (Carcharhiniformes) from the Indo-West Pacific, with Description of a New Species. *Fishes* 9, 121.
- Wright, J., Colling, A., 1995. *Seawater: Its Composition. Properties and Behavior*, Pergamon, Oxford.
- Wright, J., Seymour, R.S., Shaw, H.F., 1984. REE and Nd isotopes in conodont apatite: variations with geological age and depositional environment. In: Clark, D.L. (Ed.), *Conodont Biofacies and Provincialism. Geol. Soc. Am. Spec. Pap.*, vol. 196, pp. 325–340.
- Zhang, L., Algeo, T.J., Cao, L., Zhao, L., Chen, Z.-Q., Li, Z., 2016. Diagenetic uptake of rare earth elements by conodont apatite. *Palaeogeogr. Palaeoclimatol. Palaeoecol.* 458, 176–197.
- Zhao, L.S., Chen, Z.Q., Algeo, T.J., Chen, J.B., Chen, Y.L., Tong, J.N., Gao, S., Zhou, L., Hu, Z.C., Liu, Y.S., 2013. Rare earth element patterns in conodont albid crowns: evidence for massive inputs of volcanic ash during the latest Permian biocrisis? *Glob. Planet. Chang.* 105, 135–151.
- Žigaitė, Ž., Qvarnström, M., Bancroft, A., Pérez-Huerta, A., Blom, H., Ahlberg, P.E., 2020. Trace and rare earth element compositions of Silurian conodonts from the Vesiku Bone Bed: histological and paleoenvironmental implications. *Palaeogeogr. Palaeoclimatol. Palaeoecol.* 549, 109449.